Decomposing oceanic temperature and salinity change using ocean carbon change

Charles E. Turner[1], Peter J. Brown[2], Kevin I. C. Oliver[1], and Elaine L. McDonagh[2,3]

[1]University of Southampton, European Way, Southampton, SO14 3ZH
[2]National Oceanography Centre, European Way, Southampton, SO14 3ZH
[3]NORCE Norwegian Research Centre, Bjerknes Centre for Climate Research, Bergen, Norway

Correspondence: Charles Turner (charles.turner@soton.ac.uk)

Abstract. As the planet warms due to the accumulation of anthropogenic CO_2 in the atmosphere, the ~~global ocean uptake of heat can largely be described as a linear function of anthropogenic CO_2 uptake. This relates the oceans mitigation of atmospheric warming and carbonsequestration, as well as its increasing heat content~~interaction of surface ocean carbonate chemistry and the radiative forcing of atmospheric CO_2 leads to the global ocean sequestering heat and carbon, in a ratio that is near constant in time. This ratio has been approximated as globally uniform, enabling the intimately linked patterns of ocean heat and carbon uptake to be derived. Patterns of ocean salinity also change as the earth system warms due to hydrological cycle intensification and perturbations to air-sea freshwater fluxes. Local temperature and salinity change in the ocean may result from perturbed air-sea fluxes of heat and freshwater (excess temperature, salinity), or from ~~variability resulting from~~ reorganisation of the preindustrial temperature and salinity fields (redistributed temperature, salinity), which are largely due to circulation changes. Here, we present a novel method in which ~~by tracking~~ the redistribution of preindustrial carbon ~~, we may estimate~~ is diagnosed, and the redistribution of temperature and salinity estimated using only local spatial information. We demonstrate this technique ~~by estimating the redistribution of heat and salinity~~ in the NEMO OGCM coupled to the MEDUSA-2 Biogeochemistry model under a RCP8.5 scenario over 1860-2099. ~~We find on the longest timescales, the patterns of excess heat and salinity storage are dominated by increases in excess heat and salinity in the Atlantic, and that excess salinity~~ The excess changes (difference between total and redistributed property changes) are thus calculated. We demonstrate that a global ratio between excess heat and temperature is largely appropriately regionally with key regional differences consistent with reduced efficiency in the transport of carbon through the mixed layer base at high latitudes. On centennial timescales, excess heat increases everywhere, with 25±2% of annual global heat uptake in the North Atlantic over the 21st century. Excess salinity meanwhile increases in the Atlantic but is generally negative in other basins, ~~compensating for strong~~ consistent with increasing atmospheric transport of ~~excess salinity to the Atlantic~~freshwater out of the Atlantic. In the North Atlantic, changes in the inventory of excess salinity are detectable in the late 19th century, whereas increases in the inventory of excess heat does not become significant until the early 21st century. This is consistent with previous studies which find salinification of the Subtropical North Atlantic to be an early fingerprint of anthropogenic climate change.

~~We also find~~ Over the full simulation, we also find the imprint of AMOC slowdown through significant redistribution of heat away from the North Atlantic, and of salinity to the South Atlantic~~, consistent with AMOC slowdown. Temperature~~

change at depth . Globally, temperature change at 2000m is accounted for predominately by redistributed , rather than both by redistributed and excess heat, but the opposite is true for salinity , where for salinity the excess component accounts for the majority of changes at depth. the surface and at depth. This indicates that the circulation variability contributes significantly less to changes in ocean salinity than to heat content.

Though by By the end of the simulation excess heat is the largest contribution to density change and steric sea level rise, the storage of while excess salinity greatly reduces variability in excess density spatial variability in steric sea level rise through density compensation of excess temperature patterns, particularly in the Atlantic. HereIn the Atlantic, redistribution of the preindustrial heat and salinity fields also produce generally opposing compensating changes in sea level, though patterns are this compensation is less clear elsewhere.

As expected, the The regional strength of excess heat and salinity signal grows through the model run in response to the evolving forcing. In addition, the regional strength of the redistributed temperature and salinity signals also grow, indicating increasing circulation variability or systematic circulation change on timescales of at least the time scale of the model run.

1 Introduction

The planet continues to warm due to As a result of continuing anthropogenic CO_2 accumulation in the atmosphereemissions, atmospheric CO_2 levels continue to increase, as well as global mean surface air temperatures. However, the ocean acts to mitigate climate changeboth changes, having absorbed a third of all CO_2 emissions to date (Khatiwala et al., 2013), as well as over 9093% of the additional heat accumulating in the Earth system (Church et al., 2011). Though this greatly slows the rate of surface warming, it is not without consequence: as a result of the excess heat content, global sea levels are expected to rise significantly over the coming centuries, in large part due to the thermal expansion of seawater (thermosteric sea level rise) (Pardaens et al., 2011), (Church et al., 2013), with enormous implications for future economic development (Hinkel et al., 2014). It also has important implications for the future of marine ecosystem health: ocean warming has a direct effect on marine life as a driver of deoxygenation (Oschlies et al., 2018), as well as through increased stratification (Gruber, 2011). The uptake of carbon similarly affects marine life through its role in ocean acidification (Gruber, 2011).

The ocean heat and carbon uptakes are intimiately linked through the radiative forcing of CO^2 and the oceans ability to sequester As a result of the interaction of ocean biogeochemistry with rising atmospheric CO_2 (Bronselaer and Zanna, 2020) , (Goodwin et al., 2015), resulting in and the increased radiative forcing it generates, there exists a near linear relationship between the response of the ocean to increasing atmospheric temperatures and CO_2 levels. This allows us to leverage our understanding of changes to the ocean carbon cycle to study changes in ocean heat content and circulationglobal mean surface air temperature change and cumulative carbon emissions, known as the Transient Climate Response to cumulative Carbon Emissions (TCRE) (Goodwin et al., 2015), (Katavouta et al., 2018). A similar near-linear global relationship exists between increases in ocean heat and carbon content (Bronselaer and Zanna, 2020), which can be observed at a range of scales: both increases in global ocean heat and carbon inventories, and in local ocean temperature and carbon are linearly related.

The warming earth system also drives changes in the hydrological cycle - consequent regional variability in ocean salinity driven by Local ocean heat content changes are contributed to by both the addition or removal of heat from the surface due to perturbed radiative forcing (excess heat), or from the rearrangement of the preindustrial temperature field from circulation variability (redistributed heat). Ocean salinity changes can also result from perturbations to air-sea freshwater fluxes (such as evaporation and precipitation)is described here as the excess salinity field . Regional variability in temperature and salinityis also driven by reorganisation of the excess salinity), or due to the rearrangement of the preindustrial salinity field (redistributed salinity).

The redistribution of temperature and salinity field, such as by circulation changes, described here as redistributed variability . In the past the redistributed components of change have dominated over the excess (Zika et al., 2021), (Bronselaer and Zanna, 2020) but the excess temperature field will become increasingly important in the future, while the excess salinity field is less well understood and studied. Regional sea level rise is impacted by not only by the local component of excess temperature , but also local excess salinity, redistributed temperature change, and redistributed salinity change. Thus it is important to understand the character, distribution and evolution of excess and redistributed temperature and salinity in order to understand their contributions to as a result of ocean circulation variability acts on much shorter timescales than the accumulation of excess heat and salinity. Circulation-related variability comprises the majority of temporal variability in contemporary ocean temperature and salinity, (Bindoff and Mcdougall, 1994), (Desbruyères et al., 2017) and regional sea level change.

However, in order to reduce uncertainty in our estimates of local, rather than global, sea level rise, it is necessary to understand the causes of local ocean heat content and salinity changes, in a process similar to the identifications of anthropogenic carbon (C_{anth} in the ocean : changes to ocean circulation are (Church et al., 2013). However, the excess component is anticipated to dominate in the future (Bronselaer and Zanna (2020), Zika et al. (2021)). Thus the evolution of excess temperature and patterns of excess salinity as well as changes in ocean circulation comprise a key source of uncertainty in estimates of regional sea level rise estimates Church et al. (2013)(Church et al., 2013).

It While it remains challenging to separate the nature of anthropogenically (or naturally) forced temperature and salinity change in the ocean as we do carbon . While increased carbon content does not alter ocean circulation, changes in the temperature and salinity structure do.As a result, observed temperature and salinity excess and redistributed (preindustrial) heat, a similar decomposition for carbon is widely used. Identifying whether changes in ocean dissolved inorganic carbon (DIC) content are due to increased atmospheric CO_2 or changes in other processes (circulation, biological change, etc.) is possible due to the fact that atmospheric CO_2 can considered to be globally uniform, and biogeochemically-driven DIC changes may be due to the addition or removal of heat or freshwater (known as excess heat/salinity, and associated with increased radiative forcing)or the rearrangement of the existing temperature/salinity field (known as redistributed heat/salinity). Though distinguishing between these two 'types' of temperature/salinity change is difficult observationally, they are theoretically distinct, and contributed very differently to ocean changes as the planet warms. With the exception of basal ice shelf melt, excess heat and salinity must invade the ocean through the surface, and so significant accumulation of large quantities of excess heat and salinity by the ocean is well represented by the steady state advection of a boundary condition. However, the redistribution of temperatureand salinity by the ocean in response to circulation variability acts on much shorter timescales, and

contributed the majority of variability in contemporary ocean temperature and salinity when approximated using a spice-heave decomposition (Desbruyères et al., 2017), (Bindoff and Mcdougall, 1994). Identifying whether changes in ocean temperature and salinity are due to excess or the redistribution of the preindustrial fields therefore has implications for understanding timescales of sea level rise, as well as both short and longer timescale variability in ocean temperature and salinity.

A similar decomposition may be applied to the increased ocean carbon content: the total dissolved inorganic carbon (DIC) may be separated into two pools: Natural Carbon (C_{nat}, the DIC which would be found in the global ocean if atmospheric CO_2 were to remain at preindsutrial levels, and Anthropogenic Carbon (parameterised. This allows us to separate changes in DIC into changes in anthropogenic carbon (C_{anth}, which enters the ocean as a result of this increasing atmospheric CO_2. However, the DIC content considered to be due to increased atmospheric CO_2 changes, unlike temperature of freshwater flux changes, are approximately globally uniform meaning DIC change can be partitioned into changes in $_2$), and changes in natural carbon (C_{nat} changes and those of , defined to be the non-C_{anth} (Gruber et al. (1996), Touratier and Goyet (2004), Vázquez-Rodríguez et al. (2009), Hall et al. (2002), Khatiwala et al. (2005)). part of DIC) (Gruber et al. (1996), Hall et al. (2002) , Touratier and Goyet (2004), Khatiwala et al. (2005), Vázquez-Rodríguez et al. (2009)). Natural carbon is therefore the sum of the pools of saturation carbon, carbonate carbon, soft tissue carbon and disequilibrium carbon: it can be thought of as the DIC field which exists in the ocean, prior to the Industrial Revolution (Williams and Follows (2011)), McKinley et al. (2017), Couldrey et al. (2019)). Although not precisely identical, the decomposition of DIC into natural and anthropogenic components can provide valuable insights into excess and redistributed carbon (Williams et al., 2021). Unlike carbon however, it is not straightforward to separate anthropogenically-driven changes in ocean temperature or salinity, due to the non-globally uniform nature of the perturbations: this has motivated a variety of techniques which aim to decompose excess and redistributed heat content changes.

Though decomposition of DIC into C_{nat} and C_{anth} signals remains imperfect (estimates of local C_{anth} concentrations can differ significantly depending on the choice of reconstruction (Khatiwala et al., 2013), it is far more developed than that of decomposing temperature or salinity changesOne approach to determine excess temperature is to use a Passive Anomalous Tracer (PAT), which obeys the same physics as temperature, but is defined to have a preindustrial field which is zero everywhere: the preindustrial field therefore cannot contribute to redistribution (Banks and Gregory (2006), Gregory et al. (2016)), and so PAT reveals the distribution and evolution of the excess temperature field. Alternatively, it is possible in simulations to force ocean circulation to obey preindustrial dynamics despite increasing radiative forcing: this gives a similar result, though differing by a second order term to the PAT implementation (Winton et al., 2013).

While these methods have been very informative they are only applicable to models: no real world PAT tracer exists and while transient tracers such as chlorofluorocarbons are a close analogue their interpretation in terms of excess temperature necessitates the determination of a excess temperature boundary condition. This motivates the development of proxy methods, which aim to diagnose the excess and redistributed temperature from other tracers and might be more generally applied. The approach of Bronselaer and Zanna (2020) is an example of this: by approximating the distribution of excess temperature with that of anthropogenic carbon, they are able to leverage the mechanistic coupling relating excess heat accumulation to anthropogenic carbon accumulation to produce estimates of the scale and patterns of excess heat uptake.

Using an alternative carbon based methodology, Williams et al. (2021) explains differences in storage of heat and carbon in terms of two components: 1) the correlation of excess heat and carbon (both increase over time), and 2) anticorrelation of redistributed heat and carbon (the preindustrial distributions of temperature and carbon are inverted due to the inverse temperature dependence of carbon dioxide solubility). They use this to diagnose excess and redistributed heat (note Williams et al. (2021) refer to this as added heat, though the definitions used are identical). Bronselaer and Zanna (2020) can therefore be thought of as specifying the character of this positive correlation between excess heat and anthropogenic carbon, in order to estimate excess heat directly from anthropogenic carbon. Here, we introduce an approach which builds on this, specifying the character of the anticorrelation between redistributed heat and natural carbon locally via the preindustrial ocean state. This allows us to ~~use C_{nat} change as a proxy for the redistribution of preindustrial temperature and salinity: redistribution leaves the properties of a parcel of water unchanged, and so we can track the redistributionof temperature and salinity using the redistributionof C_{nat}. Our method relies only on knowledge of local spatial relationships between temperature or salinity and carbon, rather than a mechanistic relationship (Bronselaer and Zanna, 2020) between~~ estimate redistributed heat (and other parameters) directly from redistributed carbon, which we approximate using natural carbon. As natural carbon is strongly anticorrelated with temperature throughout the ocean, and can be usefully assumed to change only due to redistribution, it is an ideal tracer with which to estimate temperature redistribution.

The benefit of this approach is that specifying the character of the relationship between the excess components of temperature and DIC change, as done by Bronselaer and Zanna (2020), relies on a global biogeochemical relationship derived from the radiative forcing of ~~atmospheric~~ CO_2 and the ~~oceans ability to sequester CO_2.~~ ocean carbon buffer factor: making it only applicable to temperature. In contrast, in the absence of mixing, redistribution leaves the properties of a parcel of water unchanged. As a result, ~~our decomposition is not restricted to temperature change only. This allows us not only to~~ a redistribution first approach is more generally applicable, which allows us to not only produce estimates of temperature redistribution, but also ~~the first estimates (to our knowledge) or~~ new estimates of salinity, and by extension density, redistribution. Using these, we investigate the patterns of storage of excess and redistributed temperature and salinity by the global ocean.

2 Data and Methods

2.1 Model set up

We use the NEMO v3.2 OGCM (Ocean General Circulation Model) ~~(Collins et al., 2011)~~ (Madec, 2008) coupled to the MEDUSA-2 biogeochemical model (Yool et al., 2013) and the Louvain-la-Neuve (LIM2) dynamic sea ice model (Timmermann et al., 2005)~~, following a RCP8.5 climate change scenario~~. The model was configured with the ORCA1 grid with a nominal 1 degree resolution and 64 vertical levels (Madec and Imbard, 1996). The model was spun up for 900 years, before three 240 year simulations spanning 1860-2099 were spawned: a control run (CTR), coupled climate change run (COU), and a 'warming only' run (RAD)~~.~~

~~The climate change run utilises surface flux output from a~~ , following the convention of Schwinger et al. (2014), Rodgers et al. (2020) . The ocean model was forced with output from the HadGEM2-ES (Collins et al., 2011), an earth system model ~~simulation,~~

~~driven following a RCP 8.5 pathway. The control run was forced with~~ driven using prescribed greenhouse gas, land use and atmospheric chemistry forcing following the RCP8.5 scenario over the 1860-2099 time period. In this scenario, atmospheric CO_2 increases to over 900ppm by the end of the simulations (Riahi et al. (2011), atmospheric CO_2 in these simulations is shown in Couldrey et al. (2016), Figure 1a). Surface heat, momentum, freshwater fluxes, and atmospheric chemistry from HadGEM2-ES were used to force NEMO at 6 hourly intervals, and no restoring was used.

The CTR run is forced with the 8 repetitions of the first 30 years of ~~forcing from this simulation, and the 'warming only' run with physical forcingfrom the climate change run, but with~~ these fluxes from the HadGEM2-ES forcing, with a fixed atmospheric CO_2 ~~kept constant at~~ of 286ppm~~. This allows us to calculate~~ : no significant climate change occurs in these 30 years. The 900 year spinup for all 3 model runs was also forced using this 30 year repeat forcing.

The COU run is forced with the full 240 year output from HadGEM2-ES. The RAD run has the same physical variability as in COU including that driven by atmospheric carbon increases but the atmospheric carbon is artificially relaxed to preindustrial conditions. As the RAD run only includes changes in DIC due to physical change (circulation change and warming), rather than the ocean biogeochemical response to increased atmospheric CO_2, we can calculate this response, namely anthropogenic carbon or C_{anth}~~directly as~~ , directly from the difference of the COU and RAD runs:

$$C_{anth}(x,y,z,t) = DIC^{COU}(x,y,z,t) - DIC^{RAD}(x,y,z,t) \quad (1)$$

Natural carbon, or C_{nat}~~is then calculated as~~ , is then defined to be the total DIC content with the anthropogenic carbon contribution removed: it is therefore calculated as

$$C_{nat} = DIC^{COU} - C_{anth} - \Delta DIC^{CTR} = DIC^{RAD} - \Delta DIC^{CTR}, \quad (2)$$

where ΔDIC^{CTR} is control run drift~~. As all simulations are spawned from the same spinup, C_{nat} change, ΔC_{nat} is therefore given by~~ , equivalent to $DIC^{CTR}(x,y,z,t) - DIC^{CTR}(x,y,z,t_0)$, where t_0 is the beginning of the three simulations, 1860. Therefore by definition all DIC is natural carbon at the beginning of our simulations, as the DIC fields are identical at the beginning of all 3 runs. DIC changes are then the sum of natural and anthropogenic carbon change. As such, we decompose the local DIC content at any time in the following way (note as C_{anth} is defined to be zero at time t_0 $C_{anth} = \Delta C_{anth}$ here):

$$DIC(x,y,z,t) = DIC(x,y,z,t_0) + \Delta C_{nat}(x,y,z,t) + C_{anth}(x,y,z,t) \quad (3)$$

Changes in natural carbon, ΔC_{nat}, are thus given by the difference in DIC between the RAD and CTR runs:

$$\Delta C_{nat} = DIC^{RAD} - DIC^{CTR} \quad (4)$$

For further detail on model setup, see ~~Couldrey et al. (2019).~~ Couldrey et al. (2016) and Couldrey et al. (2019): we utilise the same simulations as these papers. We also note that Couldrey et al. (2019) compared the representation of DIC and alkalinity in these models runs to GLODAPv2 observations (Lauvset et al., 2016), finding the modelled carbon cycle to be representative of observations, and so we expect our carbon derived identification of excess temperature and salinity to also be representative.

2.2 ~~Parametrising temperature and salinity change as functions of C_{nat} change~~

2.2 Relating the redistribution of temperature and carbon

~~Here, we refer to a general tracer, Q, instead of temperature or salinity . Provided both Q and C_{nat} are defined over the same domain, we may parametrise Q in terms of C_{nat}:~~

$$Q(x,y,z,t) = Q(\mathrm{C_{nat}}) = Q(\mathrm{C_{nat}}(x,y,z,t))$$

~~Using the relationship between Eulerian and Lagrangian derivatives:~~

$$dQ = \big(\partial_t Q + \mathbf{v}\cdot\nabla Q\big)dt,$$

~~we may express the derivative of Q with respect to C_{nat}~~ Following Williams et al. (2021), the preindustrial temperature and carbon fields of the ocean are anticorrelated as a result of the strong inverse temperature dependence of carbon solubility. In contrast, the excess temperature and anthropogenic carbon fields are correlated due to the radiative forcing of atmospheric CO_2. Bronselaer and Zanna (2020) specify this correlation between excess heat and anthropogenic carbon using a time varying, globally uniform constant, which they refer to as

$$\frac{dQ}{d\mathrm{C_{nat}}} = \frac{\partial_t Q + \mathbf{v}\cdot\nabla Q}{\partial_t \mathrm{C_{nat}} + \mathbf{v}\cdot\nabla \mathrm{C_{nat}}}$$

the carbon-heat coupling or α. Here, we aim to similarly relate the redistribution of temperature and natural carbon using an analogous redistribution coefficient, which we will label κ_r. As we also decompose salinity, we will use superscripts to denote the variable we are relating to natural carbon: the temperature redistribution coefficient,κ_r^T, refers to the preindustrial spatial covariability of natural carbon and temperature, whereas the salinity redistribution coefficient, κ_r^S refers to the preindustrial spatial covariability of natural carbon and salinity. Decomposing the total temperature change,

$$\Delta\Theta(x,y,z,t) = \Delta\Theta_e(x,y,z,t) + \Delta\Theta_r(x,y,z,t), \tag{5}$$

~~It is important to note at this point that the term $dQ/d\mathrm{C_{nat}}$ is not an Eulerian derivative: it is simply a total derivative in $Q - \mathrm{C_{nat}}$ space. This leads to the result that we may estimate the total derivative $dQ/d\mathrm{C_{nat}}$ by considering timeseries of two quantities at a fixed geographic location. We now wish to use this relationship in order to decompose the nature of changes in Q.~~

~~Winton et al. (2013) break the tracer field Q and the transport field v up as follows:~~

$$\mathbf{v}Q = (\mathbf{v}_0 + \mathbf{v}')(Q_0 + Q') = \underbrace{\mathbf{v}_0 Q_0}_{Preindustrial} + \underbrace{\mathbf{v}' Q_0}_{Redistributed} + \underbrace{\mathbf{v}_o Q' + \mathbf{v}' Q'}_{Excess},$$

where ~~$\mathbf{v}_o$~~ Θ is in situ potential temperature, Δ refers to change since 1860, and the subscripts e and ~~Q_0~~ r refer to the ~~preindustrial components of $\mathbf{v}$ and Q, and $\mathbf{v}'$ and Q' the perturbations. We will refer to the term $\mathbf{v}'Q_0$ as the redistributed component, and the terms $(\mathbf{v}_0 + \mathbf{v}')Q'$ as the excess component of Q.~~ excess and redistributed components, respectively.

Following Winton et al. (2013), we split the velocity field $\mathbf{v}$, though we decompose our velocity field further:

$$\mathbf{v} = \mathbf{v_0} + \mathbf{v}' = \bar{\mathbf{v}} + \mathbf{v}_s + \mathbf{v}_l$$

The approach of Bronselaer and Zanna (2020) is therefore to parameterise $\Delta\Theta_e$ as

$$\Delta\Theta_e(x,y,z,t) = \alpha_T(\Delta t) \times \mathrm{C}_{\mathrm{anth}}(x,y,z,t), \tag{6}$$

Here, the velocity field is first split into two components: the initial,steady state component, $\mathbf{v}_0$, and the velocity anomaly field due to climate change, $\mathbf{v}'$. When considering correlations between two variables, it is necessary to split the steady state component $\mathbf{v}_0$ into the mean steady state flow, $\bar{\mathbf{v}}$, and deviations from this mean flow, $\mathbf{v}_s$, which we label the short timescale velocity anomaly. We have also relabelled $\mathbf{v}'$ to $\mathbf{v}_l$ to explicitly identify it with longer timescale variability in ocean circulation, rather than just deviations from mean flow. Whilst $\mathbf{v}_s$ is assumed to be composed mainly velocity anomalies due to seasonal variability contained in $\mathbf{v}_0$, it may also include changes to the seasonal cycle resulting from climate change.

We now define a new operator, $\bar{d}_t$ as follows:

$$\bar{d}_t = \partial_t + \bar{\mathbf{v}} \cdot \nabla = \frac{d}{dt} - \left(\mathbf{v}_l + \mathbf{v}_s\right) \cdot \nabla$$

such that $\bar{d}_t$ would be the total derivative, were circulation forced to remain in its mean preindustrial state, without seasonal variability. The time integral of this quantity therefore approximates the excess. Combining Equations (6)and (9), we obtain

$$\frac{dQ}{d\mathrm{C}_{\mathrm{nat}}} = \frac{\bar{d}_t Q + (\mathbf{v}_s + \mathbf{v}_l) \cdot \nabla Q}{\bar{d}_t \mathrm{C}_{\mathrm{nat}} + (\mathbf{v}'_s + \mathbf{v}'_l) \cdot \nabla \mathrm{C}_{\mathrm{nat}}}$$

We now show how this relationship may be leveraged to obtain estimates of excess and redistributed Q from carbon change. On short timescales, we may assume that $\mathbf{v}_s \gg \mathbf{v}_l$, and $\mathbf{v}_s \gg \bar{d}_t$ for both Q and $\mathrm{C}_{\mathrm{nat}}$: that is , short timescale variability far exceeds the accumulation of excess Q, or redistribution of Q or $\mathrm{C}_{\mathrm{nat}}$ (excess $\mathrm{C}_{\mathrm{nat}}$ is minimal by construction). On such timescales, the correlation between the two variables is therefore determined nearly entirely by their spatial covariability . We label this quantity the spatial variability coefficient, $\kappa_s$where α_T is their coefficient α, expressed in units of temperature rather than heat. α is estimated as the ratio of global heat to DIC accumulation, over the time period $\Delta t = t - t_0$, where t_0 is a preindustrial time (1860 here). Similarly, we might parameterise the redistribution of temperature, $\Delta\Theta_r$ in terms of the natural carbon change:

$$\Delta\Theta_r(x,y,z,t) \approx \kappa_r^T(x,y,z) \times \Delta\mathrm{C}_{\mathrm{nat}}(x,y,z,t) \tag{7}$$

Unlike α_T, κ_r^T is not a function of time: it is instead a function of position, as it relates the spatial covariability of the preindustrial temperature and carbon fields at a given point. This method is equally applicable to any property for which we aim to estimate redistribution although each property pair will have a distinct distribution of κ_r: we could instead choose to relate the spatial covariability of the preindustrial salinity and carbon fields. We would therefore estimate redistributed salinity,

ΔS_r, as

$$\Delta S_r(x,y,z,t) \approx \kappa_s^Q = \frac{\mathbf{v}_s \cdot \nabla Q}{\mathbf{v}_s \cdot \nabla \mathrm{C_{nat}}} {}^{S}_{r}(x,y,z) \times \Delta \mathrm{C_{nat}}(x,y,z,t), \tag{8}$$

~~On sufficiently long timescales, we may assume that seasonal variability averages to zero, and so $\mathbf{v}_l \gg \mathbf{v}_s$. Therefore, the change in Q due to redistribution (dQ_r, for which $\bar{d}_t Q_r = 0$ by definition), is given by~~

$$\frac{dQ_r}{d\mathrm{C_{nat}}} = \frac{\mathbf{v}_l \cdot \nabla Q}{\mathbf{v}_l \cdot \nabla \mathrm{C_{nat}}},$$

~~provided that~~ In Equations 7 and 8, no constraint is made such that the global integral of redistributed heat is zero (or equivalently the global mean redistributed temperature is zero). If $\mathrm{C_{nat}}$ ~~changes only through redistribution~~were a perfect tracer for redistribution, then its global integral would be zero. However, ~~due to changes in $\mathrm{C_{nat}}$ resulting from biological variability and~~ we expect the global integral of $\Delta \mathrm{C_{nat}}$ to be nonzero, predominantly as a result of the outgassing of saturation carbon, $\mathrm{C_{sat}}$ (the DIC content of the ocean resulting from equilibrium with the preindustrial atmosphere), in response to ~~warming, $\mathrm{C_{nat}}$ does not well satisfy this.~~ ocean warming. Thus the quantities $\Delta \mathrm{DIC}_r$ (redistributed DIC) and $\Delta \mathrm{C_{nat}}$ will differ, particularly over timescales of multiple decades to centuries (Williams et al., 2021): to reflect this, we have used approximate rather than exact equality in Equations 7 and 8. In general, when integrating over the global ocean,

$$\frac{d}{dt} \iiint \mathrm{C_{nat}} dV < 0, \tag{9}$$

~~and~~ so we correct for ~~this~~ the divergence of $\mathrm{C_{nat}}$ and the ideal behaviour of a redistributed preindustrial carbon field using a repartitioning factor, which we refer to as γ~~, and~~. We refer to the corrected quantity as adjusted natural carbon, $\mathrm{C_{nat}^{adj}}$. ~~Because of the imperfect representation of changes in redistribution by $\mathrm{C_{nat}^{adj}}$ due to biological changes , we~~ We use this to repartition a fraction of anthropogenic carbon into the adjusted natural carbon in order to correct for $\mathrm{C_{sat}}$ outgassing.

This repartitioning allows us to force the global integral of adjusted natural carbon changes to zero. However, because globally integrated biology driven changes in $\mathrm{C_{nat}}$ may be nonzero, we instead enforce the condition that globally integrated redistributed heat~~is zero in order to calculate γ. This is described by~~, not adjusted natural carbon, is zero. We therefore estimate the redistributed temperature field as

$$\Delta\Theta_r(x,y,z,t) = \kappa_r^T(x,y,z) \times \Delta \mathrm{C_{nat}^{adj}}(x,y,z,t) = \kappa_r^T(x,y,z) \times \Big(\Delta \mathrm{C_{nat}}(x,y,z,t) + \gamma(t) \mathrm{C_{anth}}(x,y,z,t) \Big) \tag{10}$$

where $\gamma(t)$ is a factor between 0 and 1 such that over the global ocean

$$\iiint \Delta\Theta_r dV = 0 \tag{11}$$

~~We may therefore estimate the change in Q due to redistribution, ΔQ_r, as~~

$$\Delta Q_r = S_u \kappa_s^Q \Delta \mathrm{C_{nat}^{adj}} = \kappa_r^Q \Delta \mathrm{C_{nat}^{adj}},$$

where κ_r^Q is our redistribution coefficient, equal to κ_s^Q multiplied by a scale factor S_u which accounts for uncertainty in our estimate of redistribution. This requires the condition

$$\mathbf{v}_s \parallel \mathbf{v}_l,$$

ie. the longer term velocity anomaly is parallel to the seasonal anomaly. This condition is quite restrictive, and unlikely to be observed strictly throughout the global oceanat all times. γ must be less than 1 or C_{nat}^{adj} would exceed DIC, and so would not be physically meaningful. It is constrained to be positive as historically, atmospheric CO_2 has increased from preindustrial levels and so the global C_{anth} inventory is positive. However, it is typically the case that one term in the sum $\mathbf{v} \cdot \nabla Q$ dominates due to the spatial gradients being much larger in one direction - usually $\mathbf{v} \cdot \nabla Q \approx w \partial_z Q$. In such cases, $\mathbf{v}_l$ can include relatively large contributions from the u and v components without similar components in $\mathbf{v}_s$ without issue, as these contributions will be scaled away by the much smaller gradients. In this approximation, this approach is conceptually similar to a spice-heave decomposition, but following a C_{nat} surface rather than a density surface. if the global C_{anth} inventory were negative, γ could also be negative (though greater than -1).

As with redistributed temperature, we will estimate redistributed salinity as

$$\Delta S_r(x,y,z,t) = \kappa_r^S(x,y,z) \times \Delta C_{nat}^{adj}(x,y,z,t) = \kappa_r^S(x,y,z) \tag{12}$$

We also note that we may combine Equations 10 and 12 in order to directly estimate salinity redistribution from temperature redistribution and vice versa. This follows from the property that (absent mixing) redistribution does not alter the properties of a parcel of water, and so the redistribution of natural carbon, temperature and salinity are related by the spatial covariability of their preindustrial fields. Alternatively, we may observe that the choice of C_{nat} is not unique as a tracer for which to estimate redistribution: as we previously note, we only a require a tracer which can be considered to change only through redistribution. The sum of the preindustrial temperature or salinity fields and their redistributed components both satisfy this, and so can be used to estimate redistribution of other tracers themselves.

We also note that in Equation (6) , replacing now wish to estimate our redistribution coefficients relating the change in adjusted natural carbon to changes in temperature (κ_r^T) and salinity (κ_r^S), in order to determine their redistribution. To do this, we use a statistical method, examining how the model temperature or salinity and C_{nat} with the full DIC field and Q with temperature before taking a global mean yields the approach of Bronselaer and Zanna (2020), where excess temperature is estimated from anthropogenic carbon. Thus, the two approaches can be considered to be opposite limits of the same relationship between DIC and temperature: redistributed temperature may be estimated from C_{nat}^{adj}, or excess temperature estimated from C_{anth}. fields covary on subdecadal timescales in order to estimate the covariability of their preindustrial state. It is well known that when making repeated observations at a fixed spatial location, the majority of observed changes in temperature and salinity are due to circulation variability, rather than material changes in water mass properties on subdecadal timescales (for example Bindoff and Mcdougall (1994), Firing et al. (2017)). We exploit the dominance of circulation variability on these timescales, assuming that the correlation between deviations in temperature, salinity and DIC from their mean state on subdecadal

timescales are due entirely to circulation variability. The correlations obtained allow us to estimate how circulation acts to couple changes in temperature and salinity to changes in natural carbon, at every point in the ocean.

2.3 ~~Implementation: Estimating redistribution~~

~~In order to estimate κ_r,~~ The calculation is performed as follows: in each grid cell, we use the first 100 years (1860-1959) of yearly mean ~~data from the control~~ temperature, salinity and DIC from our CTR run, binned into 10 decades. In each ~~decade~~decadal bin, the mean tracer (Θ or S and $\mathrm{C_{nat}}$) values are subtracted, ~~and the remaining deviations are~~ giving yearly Θ, S and $\mathrm{C_{nat}}$ anomalies from the decadal mean in that grid cell. We perform this decadal binning in order to preclude the possibility of any excess temperature or excess DIC contaminating our relationship as the result of models drifts or surface forcing driven variability due to the 30 year repeated forcing: though these effects should be small, they are both partitioned by the excess/redistribution decomposition into excess.

The correlations between the yearly anomalies from decadal means, for the entire 100 years of data, are then used to establish ~~a valueof κ_s~~an intermediate value, which we label κ_i, at each grid cell. This is done using ~~Principal Component Analysis PCA). It was found that correcting for model drift when estimating κ_s was detrimental to estimates, as it reduces the quality of correlations between the deviations in temperature and carbon. However, it was necessary to correct for model drifts when estimating $\mathrm{C_{nat}}$ changem as model drifts were of comparable size to the total change in $\mathrm{C_{nat}}$ over the time period.~~ a total least squares linear fit, implemented as two dimensional PCA: we estimate κ_i as the gradient of the slope obtained. We perform a total least squares fit, rather than ordinary, as we expect the two variables to be correlated, but not causally: total least squares is therefore more appropriate, as our relationship should not be affected by the choice of dependent variable.

We then calculate ~~S_u~~ a suppression factor, ϕ, based on the quality of the correlations to estimate κ_r for each variable: this process is detailed in Appendix (A)~~. Adjusted~~, along with a visualisation of the estimation process. As with κ_r, this will be unique to each variable. ϕ is designed such that where the correlations we obtain between the Θ or S and $\mathrm{C_{nat}}$ ~~was then~~ anomalies from decadal means are poor or nonexistent, no estimate of redistribution is made. As a result of this, if local $\mathrm{C_{nat}}$ changes due to biological processes but temperature or salinity due to circulation variability, our method will misclassify this as excess temperature or salinity: this also will occur at maxima/minima of temperature or salinity. However, due to the implementation of our γ correction, these misclassifications will globally integrate to zero. Over the full simulation, adjusted natural carbon increases by approximately 2μmol/kg, 0.1% of the mean preindustrial DIC concentration. This implies the net global divergence of $\mathrm{C_{nat}^{adj}}$ and $\Delta\mathrm{DIC}_r$ is approximately 0.1%.

The full calculation is therefore performed as

$$\Delta\Theta_r(x,y,z,t) = \kappa_r^T(x,y,z) \times \Delta\mathrm{C_{nat}^{adj}}(x,y,z,t) = \phi_\Theta(x,y,z) \times \kappa_i^T(x,y,z) \times \Delta\mathrm{C_{nat}^{adj}}(x,y,z,t) \tag{13}$$

for temperature, and

$$\Delta S_r(x,y,z,t) = \kappa_r^S(x,y,z) \times \Delta\mathrm{C_{nat}^{adj}}(x,y,z,t) = \phi_S(x,y,z) \times \kappa_i^S(x,y,z) \times \Delta\mathrm{C_{nat}^{adj}}(x,y,z,t) \tag{14}$$

for salinity.

Estimates of redistributed salinity are complicated in the top 200m by the impacts of freshwater dilution, leading to misattribution of excess salinity from freshwater fluxes to redistribution. To resolve this issue, we recalculate salinity redistribution using the same statistical approach to locally estimate the salinity redistribution from the redistributed temperature field: we refer to this as a two step estimation. This calculation is performed as

$$\Delta S_r^2(x,y,z,t) = \kappa_r^{T-S}(x,y,z) \times \Delta\Theta_r(x,y,z,t) = \kappa_r^{T-S}(x,y,z) \times \phi_T(x,y,z) \times \kappa_i^T(x,y,z) \times \Delta C_{\mathrm{nat}}^{\mathrm{adj}}(x,y,z,t) \quad (15)$$

where the superscript 2 in $\Delta S_r^2(x,y,z,t)$ refers to the two step estimation. κ_r^{T-S} is an estimate of the T-S curve angle, and is estimated in the same way as κ_i^T and κ_i^S: we do not apply a new suppression factor.

The two redistributed salinity estimates were then combined using a sigmoidal weighting, exchanging from the two step estimate at the surface to the one step estimate at depth with equal weight at 200m. This was not found to leave any artefacts in the estimates of salinity redistribution. This process is detailed in Appendix (B).

For temperature, approximately 80% of grid cells globally have a scale factor of 0.8-1, and we find by the end of our run, the suppression factor ϕ alters the redistributed temperature of 93% grid cells globally by less than 0.04 degrees, and 60% by less than 0.02 degrees, though the RMS mean redistributed temperature is reduced by 5%. However, the small number of grid cells producing extremely large estimates (10's of degrees of change) are effectively suppressed. We therefore estimate that the statistical nature of our method introduces a minimum uncertainty of approximately 5% into our inventories.

γ was calculated for each year using Equation (~~16~~10) to satisfy Equation (~~17), before being smoothed~~ 11): a fraction of C_{anth} was added to C_{nat} to ensure the global integral of redistributed heat is zero in each year, with the fraction representing the γ value that year. We then smooth the value of γ over a 10 year period, before adding the fraction of C_{anth} each year given by our smoothed γ value to C_{nat} to obtain our $C_{\mathrm{nat}}^{\mathrm{adj}}$ field. Over the 240 year run, γ increases from 0 to approximately 0.12, with an approximately sigmoid shape. This is shown in Appendix (C).

Once the ~~adjusted C_{nat} fields~~ $C_{\mathrm{nat}}^{\mathrm{adj}}$ field had been built, ~~the same adjusted C_{nat} field~~ it was used to generate both the redistributed temperature and salinity fields~~, using Equation 16~~: we did not recalculate a new γ value to force a zero integral of salinity redistribution ~~. We choose this approach both for consistency, and due to the nature of sea ice melt: the salinity~~ in our salinity decomposition. This approach was chosen for 3 reasons. Calculating a new γ for salinity would mean a new $C_{\mathrm{nat}}^{\mathrm{adj}}$ field, and so the evolution of the redistributed temperature and salinity fields would not be linked by the same adjusted $C_{\mathrm{nat}}^{\mathrm{adj}}$ field. In addition, the salinity of sea ice in the model (6PSU) and reduced carbon content of sea ice ~~cause~~ causes some ice melt to be captured as redistributed salinity, rather than excess. This means that we do not expect globally integrated salinity redistribution to sum to zero as we do for temperature. Finally, as globally integrated redistributed salinity is not independently constrained to be zero, this allows us to use this global integral as a check on the validity of the method.

~~Estimates of redistributed salinity are complicated in the top 200m by the impacts of freshwater dilution, leading to misattribution of excess salinity from freshwater fluxes to redistribution. To resolve thisissue, we recalculate salinity redistribution using the same κ_r approach to locally estimate the gradient of the T-S curve. We then estimate the salinity redistribution by multiplying the redistributed temperature field by this local T-S gradient: we refer to~~ Excess and redistributed density fields were then built from the decomposed temperature and salinity fields. To do this, the redistributed fields were added to the initial fields, and

redistributed density calculated using TEOS-10 (McDougall and Barker, 2011). Initial density was then subtracted for density redistribution. Excess density fields were then calculated as the difference between the redistributed density field and the total density change.

3 Results

3.1 Methodology Validation

We validate our results by comparison with previous carbon proxy based methods. The method of Bronselaer and Zanna (2020) relies on the assumption of a globally uniform α value, linking carbon and heat changes at all scales, which they refer to as the carbon-heat coupling. In comparison, our technique does not enforce global uniformity of this ~~as a two step estimation. The two estimates were then combined using a sigmoidal weighting, exchanging from the two step estimate at~~ carbon-heat coupling: a local carbon-heat coupling, $\Delta\Theta_e/\Delta C_{\text{anth}}$, is instead an output of our method. Henceforth, we will refer to the global mean carbon-heat coupling as α_T, and the local carbon-heat coupling as $\Delta\Theta_e/\Delta C_{\text{anth}}$: specifically, the local carbon-heat coupling links the anthropogenic carbon and excess heat.

As we expect the correlations between the excess components of temperature and DIC changes to be positive, and between the redistributed components of temperature and DIC changes to be negative, we can infer whether our technique reliably estimates excess heat by comparing histograms of correlations between the different components of temperature and carbon change. To do this, we compare the total temperature change to DIC change, the excess temperature change to C_{anth} change, and the redistributed temperature change to $C_{\text{nat}}^{\text{adj}}$ change (equivalent to κ_r^T in our method), for each grid cell at depths of less than 2000m in our simulations. We exclude depths greater than 2000m due to the negligible ventilation and C_{anth} beyond this depth horizon. The total change and excess component correlations are calculated as the ratio of decadal mean temperature and carbon at each grid cell for the period 2090-2099 minus the initial values in 1860. Assuming the assumption of a globally uniform α_T to be accurate, we expect to find a broad distribution of ratios of total temperature change to DIC change with both positive and negative correlations, and a narrower distribution of ratios of excess temperature change to C_{anth} change, centred about the global mean value α_T. We also expect the correlations between redistributed temperature changes and $C_{\text{nat}}^{\text{adj}}$ to generally be negative.

This is shown in Figure 1: the volume weighted histogram of each of these quantities over the upper 2000m of the ocean. The distribution of the ratio of total temperature change to DIC change (black line) is generally positive, indicating the dominance of excess temperature and DIC over redistribution over this time period and region, but is broad and encompasses both positive and negative values. Its peak value occurs at the global mean value α_T: 0.016K/μmol/kg. The peak value of the ratio of excess temperature change to C_{anth} accumulation (red line) displays a slightly lower peak value (0.012-0.014K/μmol/kg), but this peak is approximately 50% greater than that of total change ($2.1 \times 10^{16}\text{m}^3$ vs $1.4 \times 10^{16}\text{m}^3$). This implies that the assumption of a globally uniform carbon-heat coupling, α, is broadly appropriate although a large spread in values exists, and that our method reliably identifies excess heat.

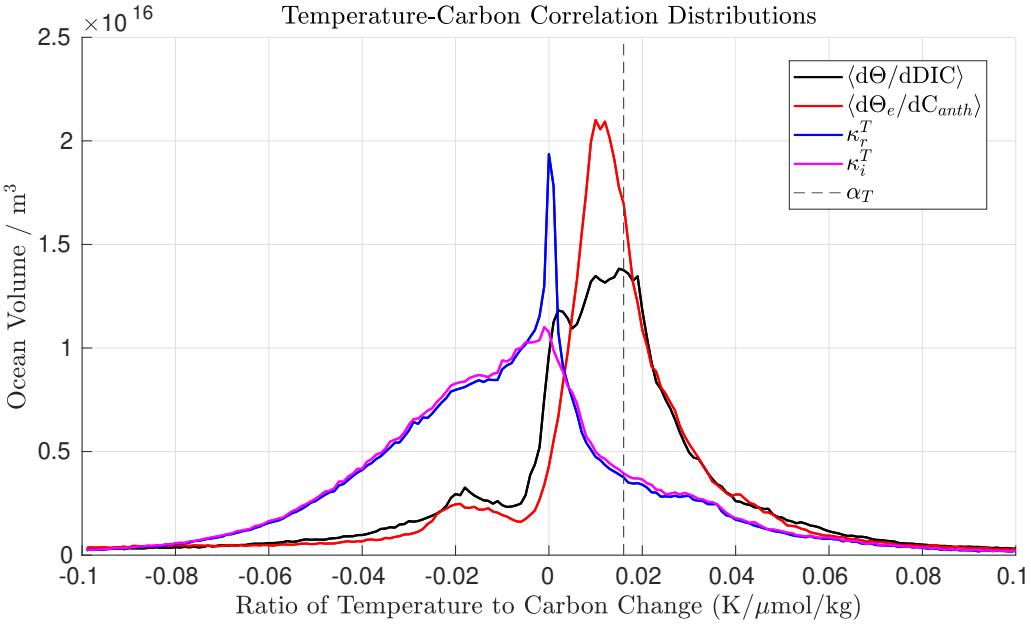

Figure 1. Histograms of the distribution of correlations relating different components of the temperature and carbon fields, over the full simulation (1860-2099). The global mean value α_T is shown by the dashed line. We include both the final redistribution coefficient, κ_r^T (blue), and its intermediate estimate, κ_i^T (magenta), as well as the ratio of total temperature change to DIC change ($\langle d\Theta/d\mathrm{DIC}\rangle$, black), and local excess temperature to anthropogenic carbon change ($\langle d\Theta_e/d\mathrm{C_{anth}}\rangle$, red).

The distribution of the ratio of redistributed temperature change to $\mathrm{C_{nat}^{adj}}$ change (κ_r^T, blue line), is also generally negative, as expected, with a much broader distribution than the distribution of the ratio of excess temperature and $\mathrm{C_{anth}}$. Generally, the ~~surface to the one step estimate at depth with equal weight at 200m. This was not found to leave any artefacts in the estimates of salinity redistribution. This process is detailed in Appendix (B)~~intermediate value histogram (κ_i^T, magenta line) resembles the final ratio (κ_r^T, blue line), with the exception of the large peak at zero, resulting from the suppression factor, ϕ_T. The positive tail of κ_r^T values is predominantly due to the inversion of the DIC field with depth in the North Pacific. That the correlation between the redistribution of temperature and carbon is positive here implies that the method of Williams et al. (2021) may not be appropriate in this location. However, the shape of our distributions are in clear agreement with their method: our decomposition infers negative correlations between redistributed temperature and natural carbon, and positive correlations between excess temperature and anthropogenic carbon, in general. As our method identifies correlations between excess temperature and anthropogenic carbon, and between redistributed temperature and natural carbon changes that are consistent with both the assumptions of Williams et al. (2021) and Bronselaer and Zanna (2020), despite not enforcing this to be the case, we have confidence that it is reliably separating excess and redistributed temperature.

~~Excess and redistributed density fields were then built from the decomposed temperature~~ We now compare estimates of excess temperature from our method and that of Bronselaer and Zanna (2020): both methods producing consistent estimates

indicates we are accurately identifying the excess temperature field. Figure 2 shows the zonally averaged excess and total temperature fields we obtain for the Atlantic and Indo-Pacific, for the final decade of our simulations, 2090-2099. In the Atlantic and Indo-Pacific, the estimate using the method of Bronselaer and Zanna (2020) (2a,b) produces smoother estimates than our technique (2c,d), but there are a number of common features which both techniques identify that are not due to the accumulation of excess heat. In the Atlantic, the tongue of warming at 2000-2500m depth, extending from approximately 40°N to 30°S is identified by both techniques as redistribution of the preindustrial temperature field, rather than excess heat. In addition, both techniques identify the region of warming extending from approximately 2000-4000m depth between 60°S and 40°S as redistribution, rather than excess heat. In the Indo-Pacific, both methods identify the cooling at approximately 1000m at 20°S as redistribution, rather than excess temperature. However, our method identifies the penetration of excess temperature to depth in the Southern Ocean, unlike the method of Bronselaer and Zanna (2020).

In the upper 1000m, there are significant divergences between the two techniques. To explore the sources of these differences, we compute local estimates of the quantity $\Delta\Theta_e/\Delta C_{anth}$ from our estimates of $\Delta\Theta_e$ and model C_{anth}. By comparing our locally obtained estimates with the patterns of excess heat and anthropogenic carbon uptake estimated by assuming a globally uniform α_T, we are able to show how our relaxation of the assumption of a globally uniform α_T causes our estimates to differ. This is demonstrated in Figure 3.

Figure 3a and ~~salinity fields. To do this, we add the redistributed change to the initial fields, and calculate redistributed density using TEOS-10 (McDougall and Barker, 2011). Initial density is then subtracted for density redistribution. Excess density fields are then calculated as the difference between thisfield and the total density change to avoid nonlinear effects $(\Delta\sigma \neq \Delta\sigma_e + \Delta\sigma_r)$.~~ 3b show local values $\Delta\Theta_e/\Delta C_{anth}$, presented as the zonal mean of the ratio of total excess temperature accumulated to total anthropogenic carbon accumulated, averaged over the decade 2090-2099. Figure 3c and 3d show the differences between the excess temperature estimated using our technique, and estimated using the technique of Bronselaer and Zanna (2020) , and Figure 3e, 3f shows the total C_{anth} accumulated over the same period and domain.

4 ~~Results~~

At depths of below 2000m in the Atlantic and 1000m in the North Pacific, ventilation is negligible and so despite large $\Delta\Theta_e/\Delta C_{anth}$ estimates, the two methods produce similar estimates of excess temperature. In the Southern Ocean, North Atlantic and North Pacific, we see large $\Delta\Theta_e/\Delta C_{anth}$ values, as well as nontrivial accumulation of excess temperature. We therefore find that in these regions, our estimates of excess temperature and those using the method of Bronselaer and Zanna (2020) diverge.

In general, our estimates of $\Delta\Theta_e/\Delta C_{anth}$ show a large degree of spatial coherence, despite no constraints being imposed to enforce this. This gives us confidence that these variations are likely real, rather than an artifact of our estimation technique. An implication of this is that heat uptake is intensified, relative to C_{anth} uptake, in the high latitude Northern Hemisphere, and reduced in the low latitude Northern Hemisphere and Southern Hemisphere. We suggest that this may be explained in terms of a reduction of carbon export through the mixed layer at high latitudes. Bronselaer and Zanna (2020) make an argument for

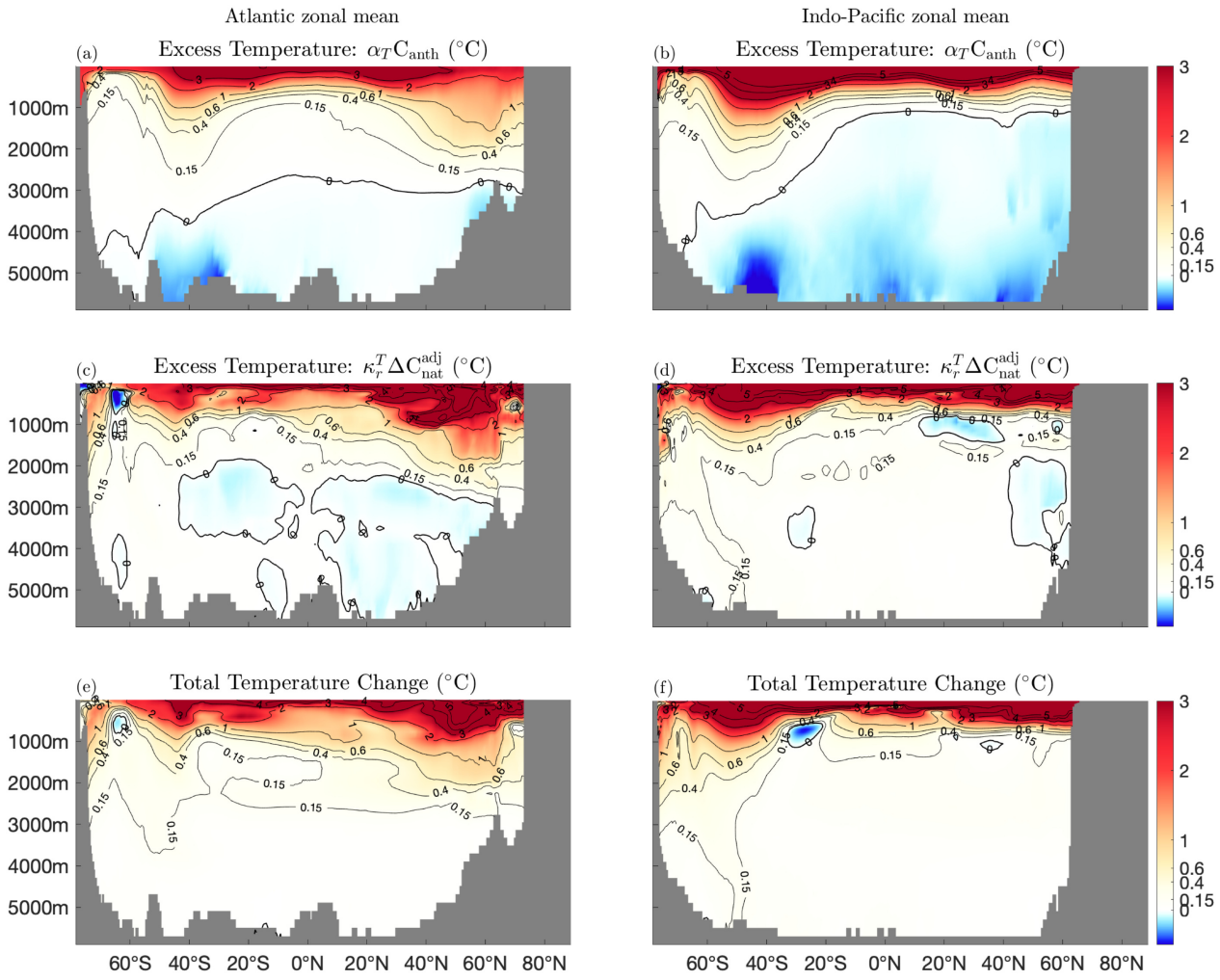

Figure 2. Atlantic and Indo-Pacific zonal, decadal mean excess temperature estimates, for the decade 2090-99, and total temperature change. The method of Bronselaer and Zanna (2020) is shown in panels (a,b), our method in panels (c,d), and the total temperature change in panels (e,f). The thick black contour indicates the zero contour, and temperature changes are indicated by thin contours, which are also indicated on the colour axes.

a globally uniform α value based on surface carbonate chemistry. However, Bopp et al. (2015) found total C_{anth} subduction through the base of the mixed layer to be significantly more variable than air-sea C_{anth} fluxes, and generally reduced at high latitudes (their Figure 3c): this mechanism could potentially act to reduce the spatial uniformity of α below the base of the mixed layer. In particular, water masses where the effects of advection and vertical mixing on carbon subduction are in opposition (namely high latitudes) tend to produce higher values of $\Delta\Theta_e/\Delta C_{anth}$.

To test whether these variations in local values of $\Delta\Theta_e/\Delta C_{anth}$ may constitute a source of error in the method of Bronselaer and Zanna (2 , we also compare the column inventories of excess heat uptake over the top 2000m of the ocean obtained using both methods in our simulations: this is shown in Figure 4. Bronselaer and Zanna (2020) were able to directly compare their estimates of excess heat and the simulated excess heat (their Figure 3f). We find that though our estimates do differ, these differences (Figure 4c) closely resemble those between their method and the simulated excess (their 3f). The zonally integrated difference in upper 2000m excess heat content (Figure 4d) is again consistent with a reduction of carbon export through the mixed layer base at high latitudes.

As our method produces results broadly consistent with both the method of Bronselaer and Zanna (2020) and Williams et al. (2021) , we believe it is reliably identifying excess temperature. In addition we find a plausible explanation for differences between the results of the two methods, that is consistent with the inference that the spatial variability in the ratio of C_{anth} and excess heat accumulation is realistic.

3.1 Inventory Changes

Global mean excess and redistributed salinity change, as well as globally integrated excess and redistributed heat content change are shown in Figure ~~1: excess components are shown in black, and redistributed components in red.~~ 5. The global mean excess and redistributed salinity (thick lines, Figure ~~1a~~5a) begin to decrease ~~immediately, though this~~ in 1891, when the RAD and CTR forcing ceases to be identical, though this sea ice melt driven decrease is much smaller than the scale of either the positive and negative only excess or redistributed salinity components (thin dashed lines): global mean excess and redistributed salinity both decrease by approximately 0.001PSU over the full run. Globally integrated excess heat does not begin to accumulate significantly until approximately 2000: until this point, both positive only (global integral of excess heat content only in regions where excess temperature is positive) and negative only excess and redistributed heat are of similar scales. Positive only excess heat and globally integrated excess heat are approximately the same by 2050, and negative only excess heat increases from approximately -200ZJ in 2000 to approximately -50ZJ by 2100: some negative excess heat due to cooling in the first half of the run remains throughout the full simulation.

The global integral of positive and negative only regions are useful for assessing the extent of redistribution: whilst the global integral of redistributed temperature is constrained to be zero, this is the result of the cancellation of the positive and negative regions. Whilst excess heat begins to dominate during the mid 21st century, the extent of temperature (and salinity) redistribution continually increases: there is no indication of 'settling' into a new circulation state, where redistribution ceases to increase, on ~~these timescales, and further additions of excess heat continually act to change the circulation. This is in agreement with previous studies, which find excess heat becoming dominant on similar time horizons. We find the global mean~~

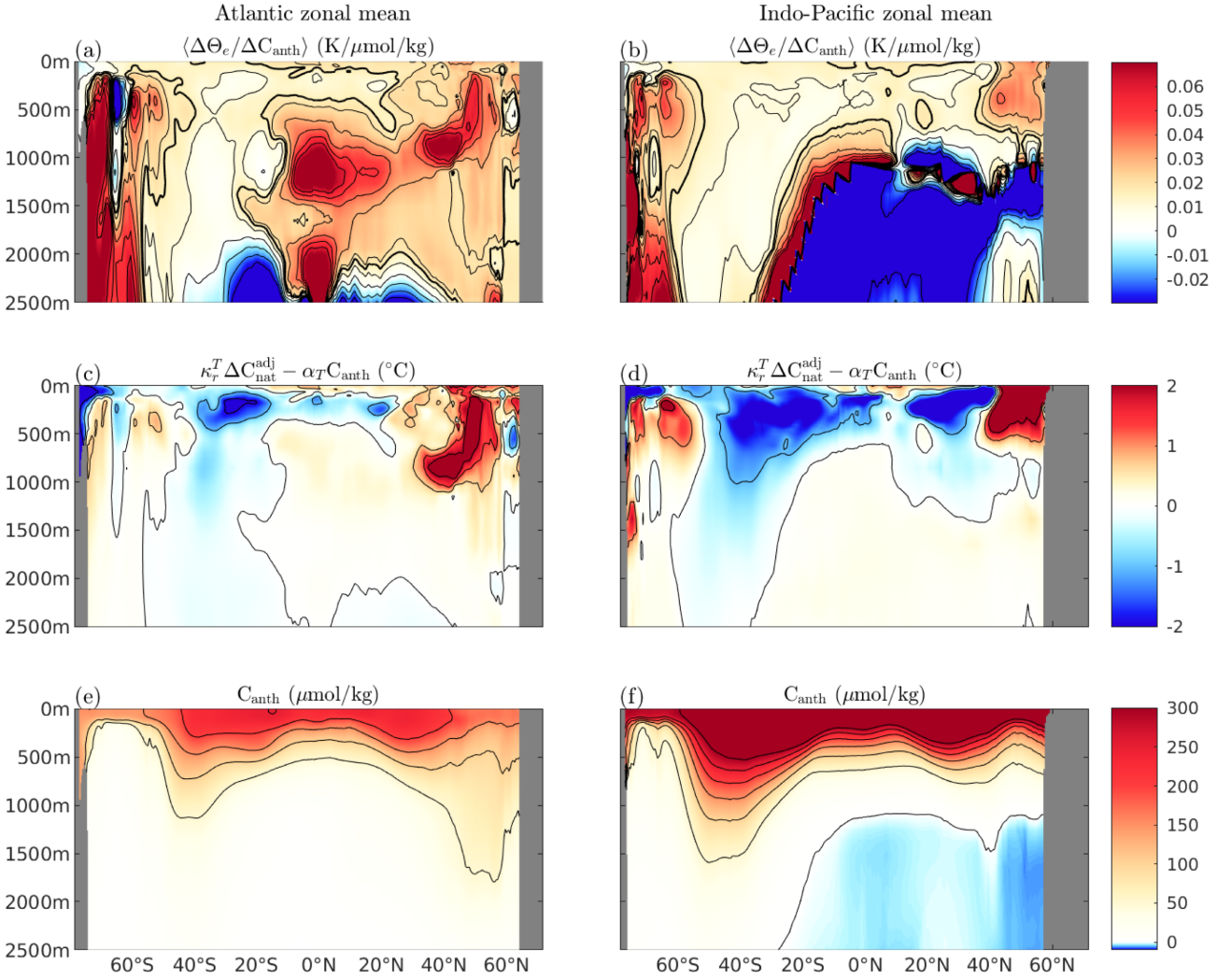

Figure 3. Atlantic and Indo-Pacific zonal mean ratio of excess temperature to C_{anth} accumulation, calculated as the 2090's decadal, zonal mean temperature divided by 2090's decadal, zonal mean C_{anth} (Panels (a), (b)). Panels (c) and (d) show the difference between our excess temperature estimate and the excess temperature estimate produced using the method of Bronselaer and Zanna (2020), and Panels (e) and (f) the zonal mean C_{anth} accumulation, calculated as the 2090's decadal mean. The thick black contour in Panels (a), (b) indicate the global mean value of α_T of 0.016K/μmol/kg, and the thin contours are indicated on the colour axes.

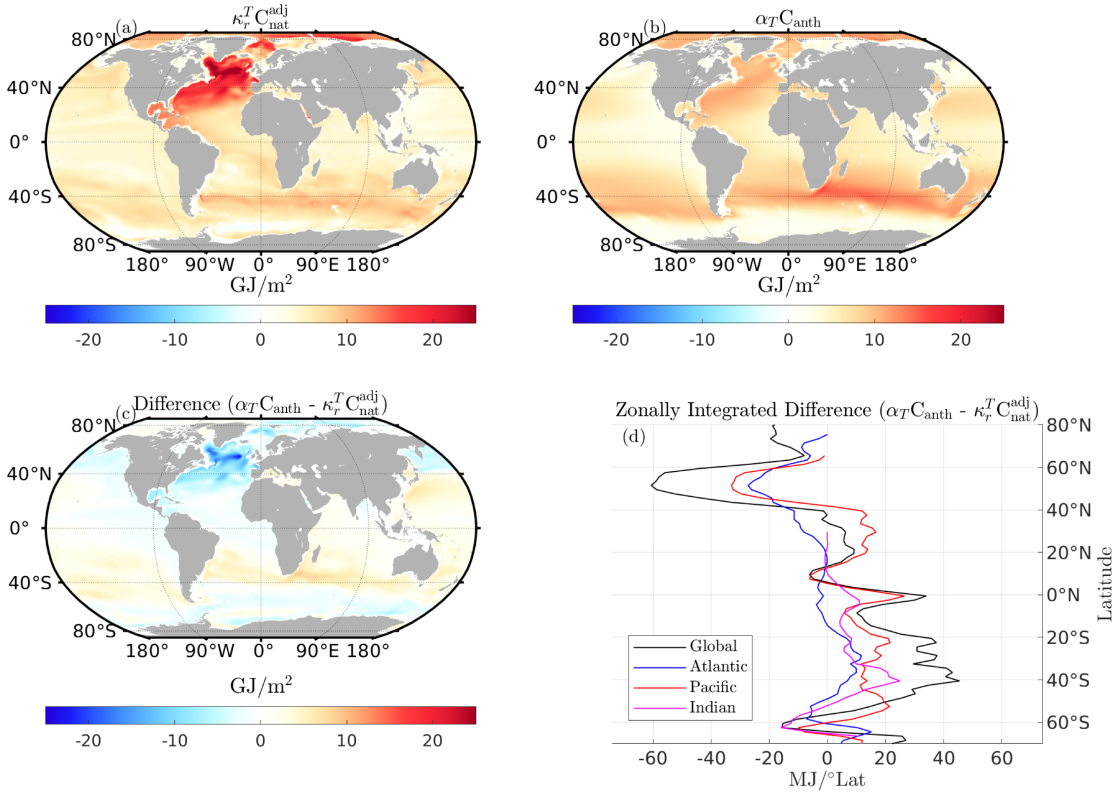

Figure 4. Column inventories of excess heat (0-2000m), calculated as the 2090-2099 decadal mean excess temperature relative to preindustrial. Panel (a) shows our method, panel (b) the method of Bronselaer and Zanna (2020), and panel (c) the difference between the two estimates. Panel (d) shows the zonally integrated upper 2000m excess heat content difference.

~~excess temperature exceeds the global mean absolute redistributed temperature in the late 2020's. Though a crude metric which does not consider differences in spatial distributions, this indicates that~~ the timescale of the ~~dominance of excess temperature is likely to occur in the near future~~full simulation. This can be seen from the continued and accelerating increases in positive and negative only redistributed heat and salinity. We also observe that whilst the magnitude of positive and negative only redistributed heat are similar until approximately 2000, excess salinity is significantly larger than redistributed salinity at all times. This indicates that during the full course of our simulations, salinity changes are dominated by changes in the freshwater cycle, rather than changes in circulation.

For comparison, we include observational estimates of ocean heat uptake from Zanna et al. (2019) (Figure 5b): cumulative heat uptake over 1871-2015 in grey (436±91ZJ) and over 1995-2015 in green (153±44ZJ). Over the period 1871-2015, our simulations underestimate cumulative heat uptake (249ZJ), but overestimate heat uptake over 1992-2015 (232ZJ).

Figure ~~2~~ 6 shows the integrated redistributed and excess temperature, salinity, and densities for each ocean basin. As with the global mean, excess salinity begins to accumulate almost immediately in most ocean basins (Figure ~~2c)~~6c), particularly the

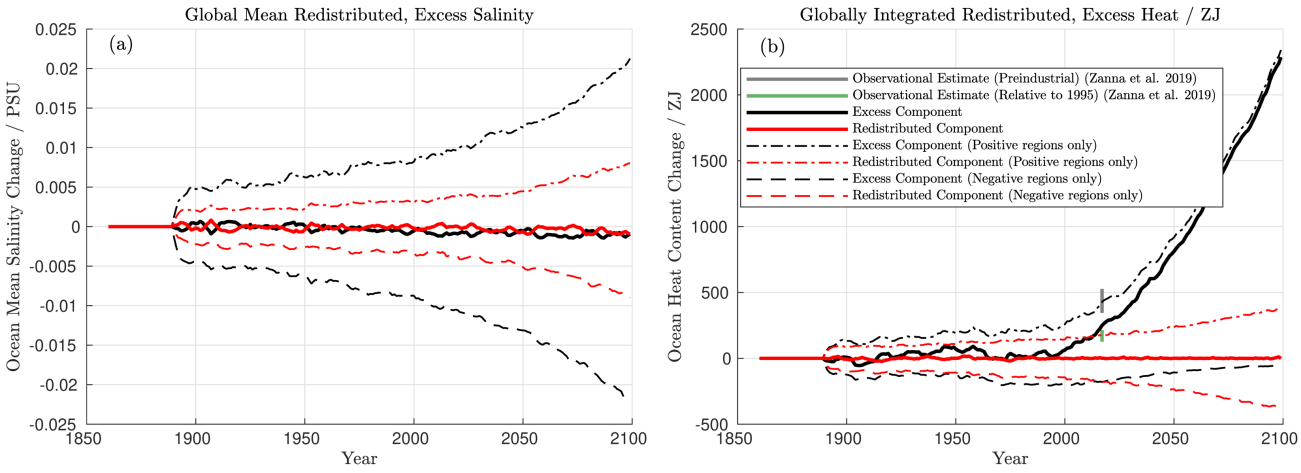

Figure 5. Global mean excess and redistributed salinity (a), and globally integrated excess and redistributed heat (b). Excess components are shown in black, redistributed components in red. The integrals of only the positive and negative regions are also shown (thin dashed lines). Climate change and control runs use the same first 30 years of forcing, so values are by definition zero here: the jump in 1890 represents the initial divergence of states. Observational estimates of global ocean heat uptake from Zanna et al. (2019) are also shown in panel (b).

North Atlantic and South Pacific: trends here are distinct from noise at 2σ in 1893 and 1911, respectively. Excess temperature ~~, with the exception of~~ does not begin to accumulate until the 21st century, at which point it begins to rapidly accumulate in all ocean basins; the exception to this is the South Atlantic (Figure 2a, dashed black line) which cools in the 20th century, ~~does not begin to accumulate until the 21st century, at which point it begins to rapidly accumulate in all ocean basins.~~ its excess heat signal emerging from noise at 2σ in 1918. In contrast, the excess heat signal in the North Atlantic and South Pacific do not emerge from noise at 2σ until 2023 and 2021, respectively. Over the period 2023-2099, for which the excess heat signal of the North Atlantic is distinct from noise, 25±2% of global excess heat accumulated is located in the North Atlantic.

The accumulation of negative excess density is dominated by the accumulation of excess temperature, rather than salinity: the grey scales on the right hand side of panels (a)-(d) show the ~~associated density change~~ density change associated with heat and salinity change. In the North Atlantic, changes in the excess heat and salinity ~~tend to~~ compensate to reduce density anomalies: a reduction of almost 25Pg associated with excess heat is compensated for by an increase of approximately 8Pg associated with increased salinity. Similar compensation, though much weaker, is seen in the South Atlantic, ~~but not~~ which cools and freshens during the 20th century before warming and salinifying in the 21st. This is not the case in other basins, where the changes in excess heat and salinity both act to decrease density and therefore increase stratification.

The redistribution of density is ~~more complicated: redistributed heatand salinity contribute on similar scales~~ less dominated by heat, with heat and salinity contributing similarly to redistributed density. In the North Atlantic, the redistribution of heat and salinity are approximately density compensated until around 2050, at which point the redistributed density ~~component~~

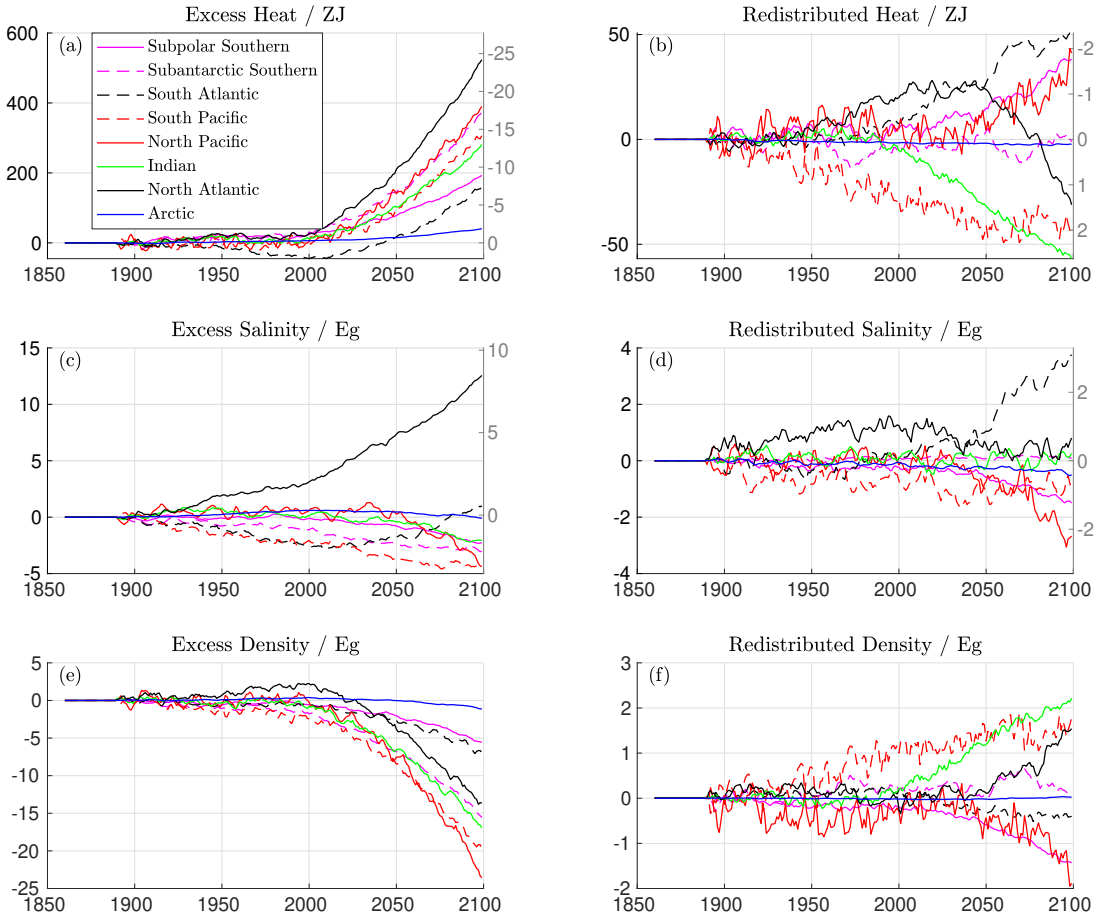

Figure 6. Excess (left column) and redistributed (right) heat, salinity and density integrals for each ocean basin over the full model run. For the changes in heat and salinity (Panels (a)-(d)), the equivalent integrated density change in units of Pg are given in grey on the right. Scales differ for excess and redistributed components, and changes in salinity and density are given as mass changes rather than volumes.

inventory begins to increase rapidly (Figure ~~2f~~6f, black line). Good density compensation in the redistributed component is also seen in the ~~Subantarctic Southern ocean~~subantarctic Southern Ocean, with minimal accumulation of redistributed density.

In our ~~climate change run, the AMOC strength~~ COU run, AMOC strength (calculated as peak depth integrated meridional volume transport at 26°N) increases until 1990 before declining continually thereafter. The cumulative transport anomaly (time integrated difference between ~~climate change and control run~~ COU and CTR AMOC volume transport) peaks in 2035 before ~~declining. This signal is particularly~~ also declining continually for the rest of the simulation. The signal of AMOC decline is visible in the redistributed heat content of the North Atlantic, which peaks in 2037 before declining rapidly, as well as

the redistributed salinity content of the South Atlantic, which begins to increase at approximately the same time~~. This is~~ : consistent with previous studies (Zhu and Liu, 2020) which find a 'pile up' of salinity in the South Atlantic as a result of AMOC slowdown. The AMOC in our simulations is too weak, with a preindustrial mean of approximately 7.5Sv at 26°N, and a maximum value of 13Sv in our COU run, declining to approximately 4.5Sv by 2099, as compared to approximately 15Sv in HadGEM2-ES (Martin et al., 2011) and 18±4.9Sv observationally (Johns et al., 2011). This AMOC strength at 26°N in HadGEM2-ES itself is towards the weaker end of estimates from CMIP5 models (Weaver et al., 2012). However, the heat transport is realistic, with a control run heat transport of 0.075PW/Sv at 26°N, as compared to observations of 0.079PW/Sv (Johns et al., 2011). The decline in AMOC strength in our ocean only simulations and HadGEM2-ES simulations are also proportional: over an RCP8.5 scenario, Sgubin et al. (2014) found a decline of AMOC strength at 26N from approximately 15.5 to 8Sv at 26°N in HadGEM2-Es.

~~As with the~~ To explicitly test whether the redistribution of heat from the North Atlantic, and salinity to the South Atlantic, can be explained in terms of a changing AMOC, we calculate the redistribution of heat and salinity through the Equator in the Atlantic. This is calculated as the difference in meridional velocities between the COU and CTR runs, multiplied by the control run temperature and salinity fields (this analysis is conceptually similar to that performed by Williams et al. (2021) in order to calculate the redistribution into/out of a volume, though here we consider only the equatorial boundary between the North and South Atlantic). For the period 1950-2099, for which there are non negligible changes in the redistributed heat content of the North Atlantic, we find the correlation between the redistributed heat content of the North Atlantic and the redistribution of heat through the Equator due to AMOC change has an R^2 value of 0.58, suggesting that the changing in overturning circulation plays a key role redistributing heat out of the North Atlantic, and into the South Atlantic. We also find a slightly weaker correlation between the non AMOC driven redistribution of heat past the equator and the North Atlantic heat inventory, with a R^2 value of 0.45. These R^2 values are reduced to 0.50 and 0.38, respectively, when considering the period 1890-2099.

The picture is similar for salinity: for the period 2000-2099, for which there are non negligible changes in the redistributed salinity content of the South Atlantic, we find a correlation between the redistributed salinity content of the South Atlantic and redistribution of salinity through the equator due to AMOC change has an R^2 value of 0.61, which is reduced to 0.04 when considering the period 1890-2099. Changes due to gyre circulation driven redistribution have R^2 values of 0.09 and 0.33, respectively, suggesting that the large scale mechanisms of salinity redistribution differ from those of heat.

As this method of calculation is able to infer redistribution directly from model outputs, we have good confidence our decomposition is reliably identifying excess heat and salinity. We therefore believe the redistribution of heat out of the North Atlantic and salinity into the South Atlantic are driven predominantly by AMOC variability, with non AMOC circulation changes influencing the redistribution of temperature and salinity differently. Identifying whether the lack of correlation between our estimates and the explicitly calculated redistribution when there is no appreciable accumulation of either is due to inaccuracies in our approach or the dominance of other factors in the redistribution of heat and salinity would likely improve our understanding of the strengths and weaknesses of this method, but is beyond the scope of this study.

As with the global inventories, we find little evidence of 'settling' into a new circulation state: ~~with the exception of~~ in most basins, redistributed heat and salinity inventories do not cease to grow during our simulations, and AMOC strength declines

continually throughout the 21st century. A notable exception is the South Pacific~~and Arctic,~~, for which the redistributed heat inventory increases to approximately -50ZJ by 2050, before remaining at a similar value for the rest of the ~~rate of accumulation of excess salinity is either unchanging or increasing throughout the run. This is less clear with redistributed heat: the emergent relationships between~~ simulation.

One way of assessing the interaction of excess and redistributed heat ~~inventories are~~ is to plot changes in their accumulation against each other, with emergent relationships consistent with coupling between the two: this is shown in Figure ~~3.~~ 7.

In the North Atlantic, we find an acceleration of the accumulation of redistributed heat with respect to the excess heat inventory (Figure 7g). However, in all other basins ~~, we find the rate of~~ for which relationships emerge clearly, the accumulation of excess ~~heat outstrips the accumulation of redistributed heat~~ and redistributed heat are either linearly related (Subpolar Southern (7a), North Pacific (7e)), or sublinear. This is as expected: the acceleration of the accumulation of redistributed heat is unique to the North Atlantic. ~~Other~~ In all basins other than the North Atlantic, the rate of accumulation of redistributed heat with respect to excess heat slows over the timeseries.

~~However, we find that of the 8 basins, only four appear to be 'saturated' with respect to redistributed heat : The subantarctic~~ Despite this slowing, the redistributed heat inventories continue to grow, except in the Subantarctic Southern, South Atlantic, South Pacific and Arctic. In all other basins, we see the continued accumulation of redistributed temperature, indicating the continual dynamic readjustment of the ocean, at an inter-basin scale: the lack of growth at a basin scale imposes no ~~constrains~~ constraints on intra-basin redistribution. Of these, the Subpolar Southern and North Atlantic are ~~perhaps~~ the most striking, with heat redistribution increasing linearly and with the square of excess heat accumulation, respectively. ~~The importance of these regions for deep and intermediate water formation indicates that the redistribution of heat by changing ocean circulation is likely to continue increasing under anthropogenic warming - we find no indication of the ocean 'settling' into a new circulation state.~~

~~It is of particular interest that the (negative) redistributed heat inventory of the North Atlantic is proportional to the square of its excess heat inventory.~~ Previous studies have found AMOC strength to be proportional to SST anomalies in the North Atlantic (Caesar et al., 2018)~~. Assuming SST anomalies~~ , and SST anomalies are thought to be proportional to excess heat (MacDougall and Friedlingstein, 2015)~~would yield such a relationship between the excess and redistributed heat in~~ . Though it would initially appear that this would act to linearly couple the excess heat content of the North Atlantic ~~. From this, we infer that~~ to the redistribution of heat out of the North Atlantic~~in our simulation is proportional to both the AMOC strength and the temperature stratification in the North Atlantic.~~

~~Expressing the ratio of the redistributed to excess heat inventories in the Atlantic north of 26N as a function of the time integrated AMOC volume transport anomaly at 26N (climate change - control run), ΔTr, we find that this ratio may be expressed as~~

$$\frac{\mathcal{H}_r}{\mathcal{H}_e} = -0.0423 + 0.0005\Delta\mathrm{Tr},$$

~~where $\mathcal{H}_r$ and $\mathcal{H}_e$ are the North Atlantic redistributed and excess heat inventories, respectively. We interpret this as the redistribution of heat southwards by an excess temperature field, even if AMOC strength were unchanged. This is counterintuitive,~~

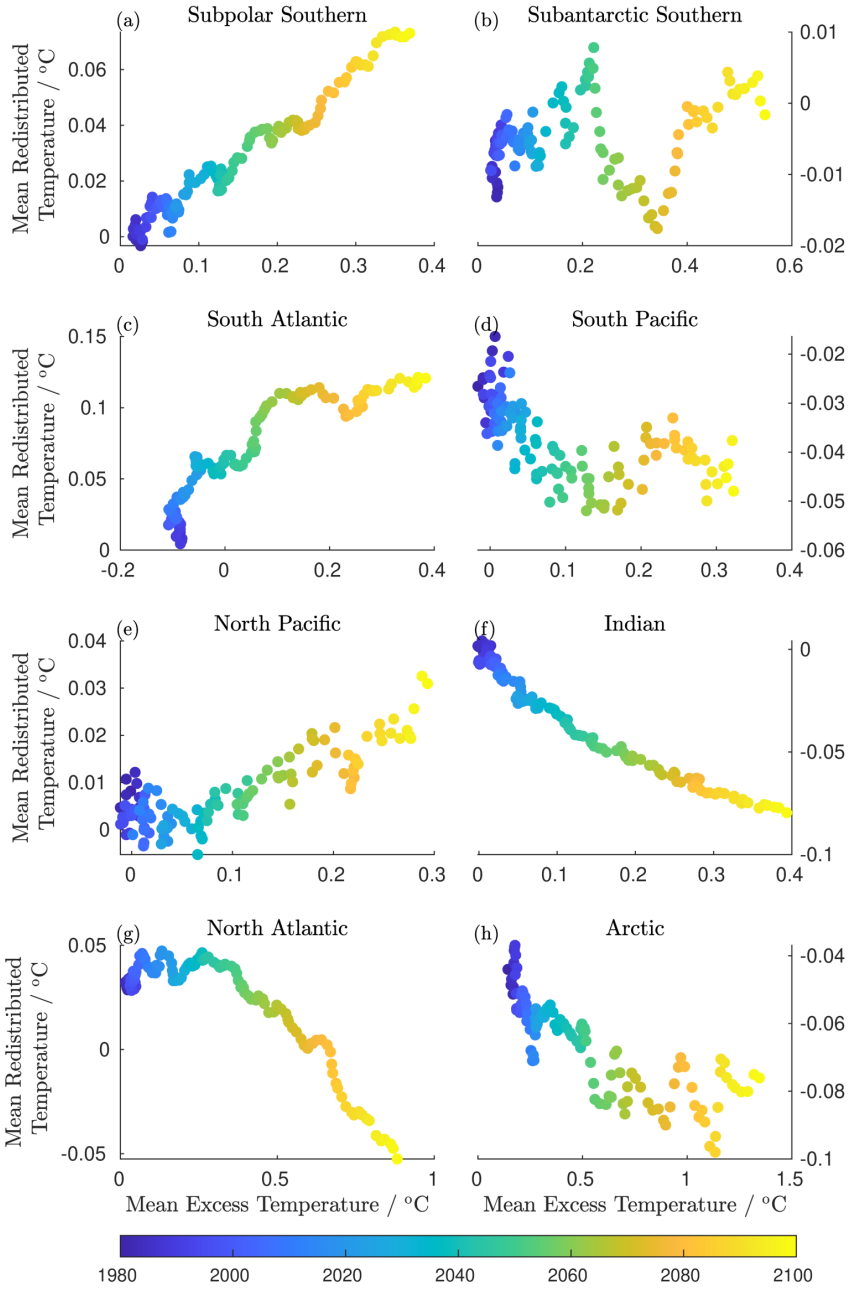

Figure 7. The emergent relationships (if any) observed between excess and redistributed heat in each of the 8 ocean basins shown in Figure ~~2.~~ 7, presented in terms of the mean redistributed and excess temperature changes for the basin. Timeseries begin in 1980 as there is no appreciable accumulation of excess or redistributed heat in the first half of the run. Scales differ for each basin.

as the AMOC transports warm surface waters northward, and cool deep waters south: we might therefore expect an increase in northwards heat transport at constant AMOC strength. However, we find the imposition of an excess temperature field acts to redistribute the preindustrial temperature field downwards, redistributing heat downwards from the northward flowing waters to those moving south. The net result is that northward heat transport is reduced, and heat is redistributed out of the North Atlantic, without any change in the overturning circulation. Finally, we note that the increasing temperature stratification , the redistributed heat inventory will be proportional to the time integrated changes in AMOC strength. The excess heat inventory of the North Atlantic increases monotonically with time, and so the rate of change of the redistributed heat inventory will be proportional to the excess heat inventory. The proportionality of the redistributed heat inventory of the North Atlantic has the unexpected result of reducing the heat transport sensitivity at 26N: we find a reduction of from in our control run to in our climate change run. We also find an excess heat transport sensitivity of averaged over the period 1980-2099, approximately accounting for this difference.

Whilst it appears from this that the AMOC transports excess heat southwards, this is not the case. Instead, a strong correlation ($R^2 = 0.68$) is observed between the decline in AMOC strength and the increasing northward transport of excess heat. Thus, the reduction in northward heat transport due to a decrease in AMOC strength is compensated for by an increase in stratification, ameliorating the reduction in northwards heat transport due to the declining AMOCto the excess heat inventory can therefore be explained in terms of the unique circulation of the North Atlantic.

3.2 Mapping storage of excess and redistributed temperature and salinity

The regional patterns of decadal mean excess and redistributed temperature for the 2090s at four depth surfaces the surface and at 2000m is shown in Figure 4, 8 and the regional patterns of the 2090s decadal mean excess and redistributed salinity in Figure 5. 9. For both temperature and salinity, surface changes are dominated in most locations by the excess component. Excess temperatures are positive nearly everywhere, whilst excess salinity is generally positive in the South Atlantic, Subtropical North Atlantic and Indian Oceans, with the Pacific generally negative. This is consistent with increased evaporation over the Atlantic and increased atmospheric freshwater transport from the Atlantic to the Pacific.

It is generally expected that in a warming climate, the hydrological cycle will become amplified, with increased evaporation (precipitation) in regions of net evaporation (precipitation) (Durack and Wijffels, 2010), (Zika et al., 2018), (Gould and Cunningham, 2021). Thus, the salty regions of the ocean surface become saltier, and the fresh regions fresher. As these changes result from changing surface fluxes, this hydrological amplification should be captured by the excess salinity at the surface, rather than redistributed salinity.: this is consistent with our results.

This behaviour is visible in the Indian ocean and in the excess salinity peaks in the Subtropical North and South Atlantic, but is far exceeded by the pattern of increasing excess salinity in the Atlantic, and reduced excess salinity in the Pacific (Figure 5a). However, the pattern of change in excess salinity at the surface strongly resembles trends in Sea Surface Salinity found by Durack and Wijffels (2010) (Figure 5) over the period 1950-2008. We infer from this that historical trends in sea surface salinity are driven predominately by excess, rather than redistributed salinity: changes in evaporation and precipitation dominate over changes in circulation. This is in agreement with our inventory estimate from Figures 1 and 2, which indicate

~~that changes to the hydrological cycle precede those of significant warming, and that the scale of excess salinity generally exceeds that of redistributed salinity at all times. Patterns of surface excess salinity in the Atlantic also strongly resemble the patterns of salinity change in response to a per decade surface heat flux found by Zika et al. (2018).~~

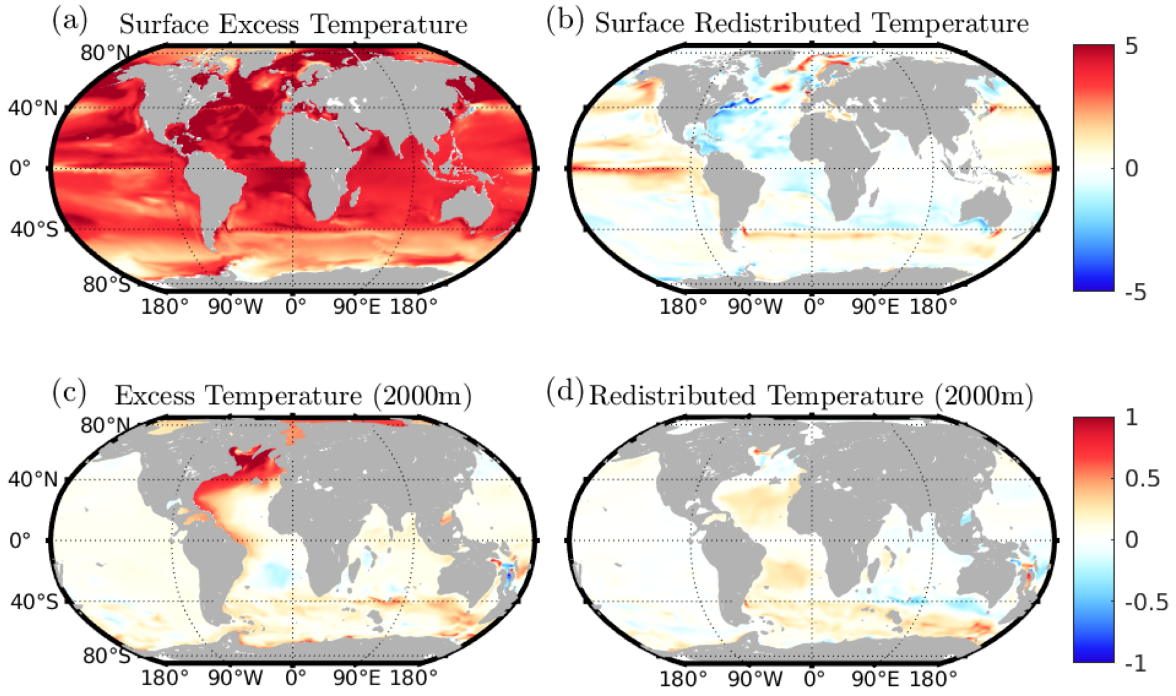

Figure 8. Maps of excess and redistributed temperature on ~~four~~ two depth surfaces: the surface ~~, 503m, 1041m~~ and ~~2097m~~at 2000m. Values given are the decadal mean for the decade 2090-2099. ~~The zero contour is shown in black, with panels (a)-(d) and (e)-(h) shading colour~~ Colour axes are shared between each component at both depths.

~~The magnitude of redistributed temperature change in general decays slowly with depth: similar values are seen at the surface and 500m, as well as at 1000 and~~ Whilst surface warming is unsurprisingly dominated by excess temperature, at 2000m ~~. In the Atlantic, at depths greater than 2100m, low latitude warming is dominated by redistributed, rather than excess temperature. In contrast, redistributed salinity change decays much more sharply with depth, with typical values approximately halving at each depth surface. Unlike temperature, at depth,~~ the contributions of excess and redistributed temperature to total temperature change are of comparable magnitude, with the exception of the North Atlantic. In contrast, the majority of salinity change at depth is accounted for by the excess ~~, rather than redistributed~~ component, though appreciable changes are generally only found in the North Atlantic. ~~However, some negative redistributed salinity is also found at depth in the North Atlantic, as well as some negative redistributed salinity at depth in the Southern Ocean.~~ This salinity increase at depth is despite surface freshening in the Subpolar North Atlantic (Figure 9a, 9c), resulting from the propagation of surface salinification here in the 20th

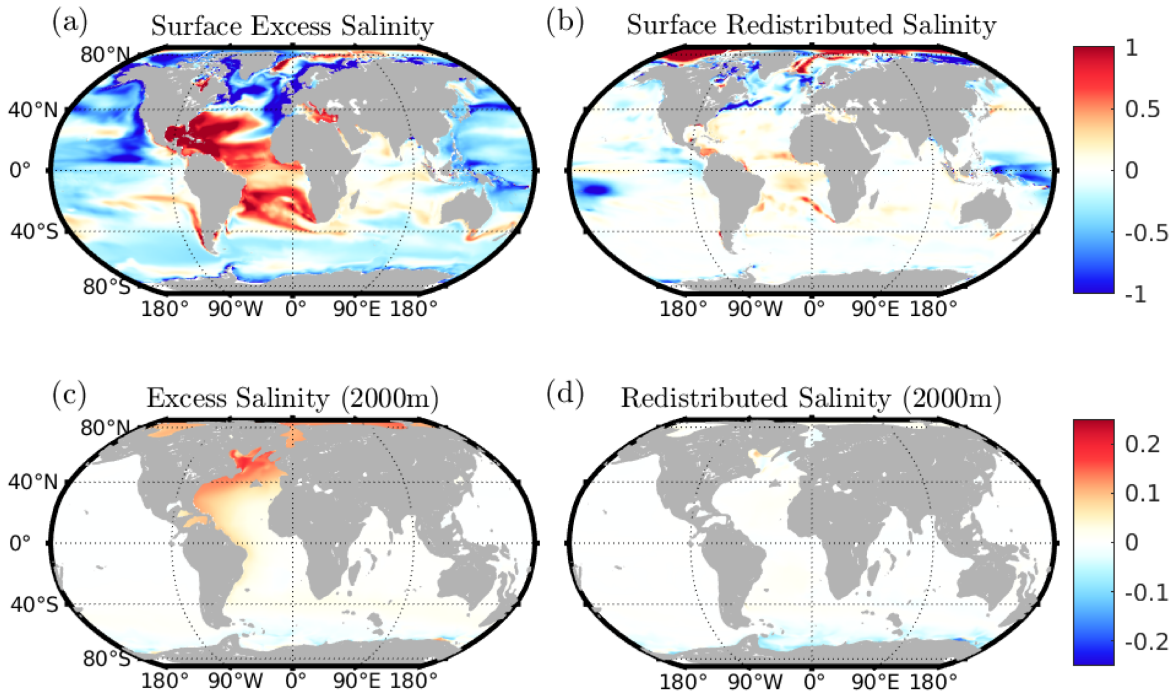

Figure 9. Maps of excess and redistributed ~~temperature~~ salinity on ~~four~~ two depth surfaces: the surface ~~, 503m, 1041m~~ and ~~2097m~~at 2000m. Values given are the decadal mean for the decade 2090-2099. ~~The zero contour is shown in black, with panels (a)-(d) and (e)-(h) shading colour~~ Colour axes are shared between each component at both depths.

century. Patterns of excess and redistributed surface salinity are consistent with the results of Sathyanarayanan et al. (2021) and Levang and Schmitt (2015).

The strong surface redistributed salinity signal in the Arctic appears to result from reduced sea ice freshwater transport from the marginal seas of the Arctic inwards. Previous studies using the NEMO GCM coupled to the LIM2 sea ice model have found that Arctic sea ice tends to grow along the coastal shelves of the Arctic Ocean, before being transported by the Beaufort Gyre circulation and transpolar drift (Moreau et al., 2016). The net result of this is to transport both freshwater and DIC from the coastal shelves to the centre of the Arctic Ocean: changes in this transport will therefore act to cause large and tightly correlated changes in DIC and salinity in the surface Arctic Ocean. Our decomposition therefore partitions salinity change resulting from changes in this transport to redistribution. Similar changes in sea ice transport also act to cause redistributed freshening in the coastal Southern Ocean.

The total inventory change in heat, salt, and density by the last decade of our simulation, as well as the storage of the excess and redistributed components are shown in Figure ~~6~~10, for the upper 2000m of the ocean. We present these as contributions to steric sea level change, allowing for both normalisation and a comparison of contributions to steric sea level rise. ~~Inventories~~

~~in native units are also presented in Figure 7. As with contributions to steric sea level rise, these are the 2090's decadal mean of each quantity for the upper 2000m. Zero contours are shown in black.~~ On this timescale, excess (Figure ~~6c, 7b~~10c) and total (Figure ~~7a~~10a) heat inventory changes are positive nearly everywhere, with the exception of the Weddell and Ross ~~gyres~~Gyres. Redistributed heat inventories are negative generally in the North Atlantic (Figure ~~6f, 7e~~10c), with the largest values seen in the Labrador and Norwegian ~~seas~~Seas, as well as the Subtropical Gyre. In the Pacific and Indian Oceans, redistributed heat inventories are ~~negative generally in the South, possibly reflecting a shift in the position of the Antarctic Circumpolar Current.Though over a different period and enforcing different assumptions, our patterns of heat redistribution are qualitatively similar to those of Bronselaer and Zanna (2020) (Figure 4), indicating both methods perform similarly.~~ most negative at around 30-35°S.

Salinity inventory changes show a ~~very~~ different geographical distribution: ~~here,~~ excess salinity increases uniformly only in the Atlantic and Arctic oceans (Figure ~~6e, 7e~~10e). Total salinity change is again dominated by the excess here. As with heat, the ~~signature~~ fingerprint of AMOC slowdown can be seen in the redistributed salinity signal: we observe redistribution driven cooling and freshening in the North Atlantic and redistribution driven warming and salinification in the Equatorial and South Atlantic, resulting from a weakening in the northward transport of heat and southward transport of fresh water. This redistribution driven cooling and freshening acts to oppose the warming and salinification associated with increased surface heating and concurrent increases in ~~Evaporation~~ evaporation - ~~Precipitation~~precipitation (E-P).

Density inventory changes (Figure 10a) are relatively globally uniform ~~(Figure 6a, 7g)~~compared to the individual contributions: a decrease is seen in the total change and excess inventory nearly everywhere, with the exception of the Weddell and Ross ~~seas~~Seas, as well as the central Arctic Ocean. The Arctic Ocean decrease is dominated by the changes in freshwater transport, whereas the Weddell and Ross ~~sea~~ Sea decrease result from upwelling cool water. In the Atlantic, large changes in steric sea level resulting from excess temperature are significantly reduced by the accumulation of excess salinity, and a similar cancellation is seen in the redistributed components.

~~The total, excess, and redistributed heat, salinity and density inventories presented as column inventories for the upper 2000m of the ocean. These quantities are calculated as the decadal mean anomalies of the 2090's relative to preindustrial. Scales are shared for each quantity.~~

4 Discussion and Conclusions

We have demonstrated a new technique for estimating the redistribution of heat and salinity by the ocean in response to anthropogenic climate change, allowing us to identify the excess signal and producing estimates consistent with other reconstructions. This method can be thought of as sitting within a family of techniques which aim to understand ocean circulation changes through the relationship between ocean temperature and DIC, along with the methods of Bronselaer and Zanna (2020) and Williams et al. (2021). It produces results which are consistent with the assumptions of both methods, without constraints to enforce this. Instead, we assume that on decadal and subdecadal timescales, local ocean heat and carbon content are dominated by redistribution, and that on longer (multidecadal to centennial) timescales, circulation variability dominates over biological

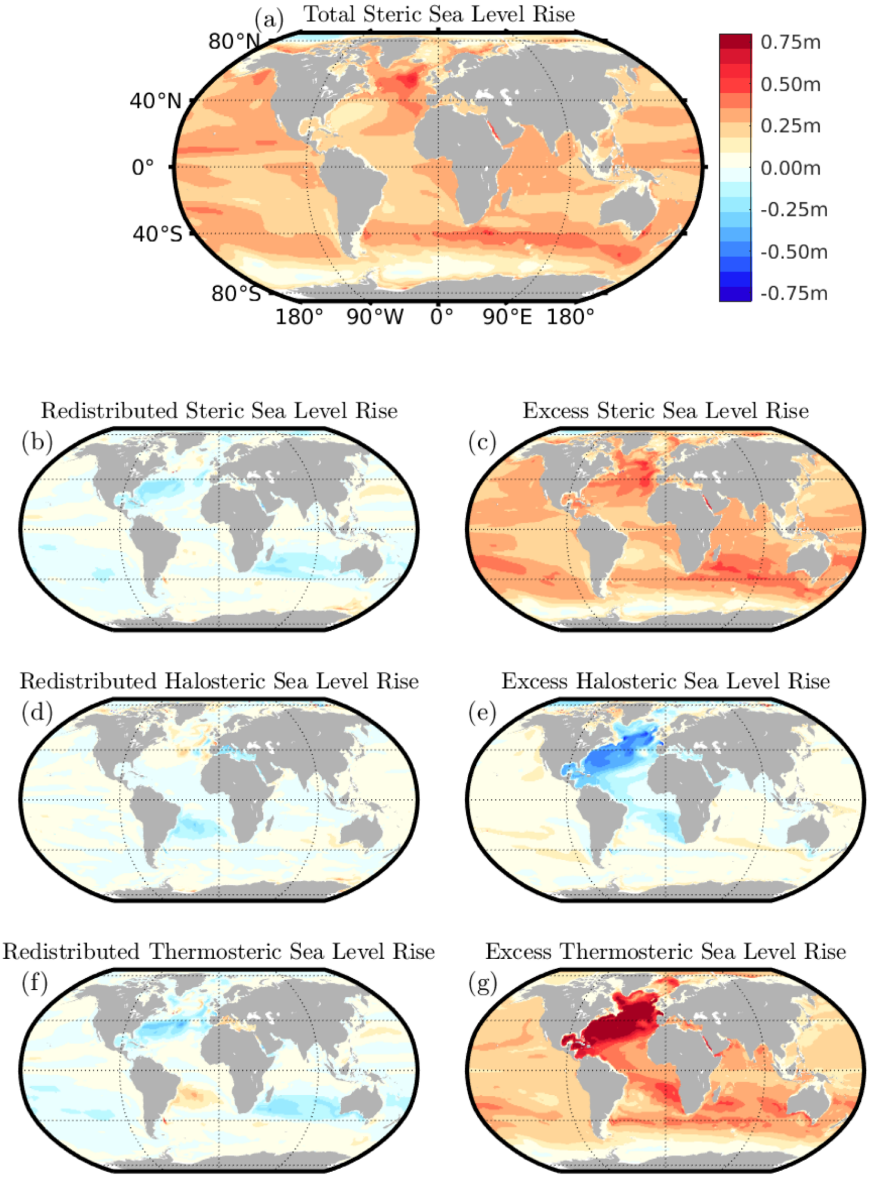

Figure 10. 2090's mean steric, halosteric and thermosteric contributions to sea level rise, as well as the total~~. Only contributions~~ , from the upper 2000m ~~are given. These can therefore also be analogously thought~~ of ~~as~~ the ~~upper 2000m inventories of the decomposed heat and salinity change~~ocean.

changes in natural carbon. This first assumption is consistent with the results of Thomas et al. (2018), who investigated the relationship between ocean heat and carbon content, finding the two to be anticorrelated on decadal timescales. The results

of Williams et al. (2021) suggest the assumption of circulation variability dominating over biologically driven changes is also reasonable. A key strength of this new technique is that it also allows us to estimate not only the redistribution of heat, but also salinity, and ~~is in principle extensible to other tracer~~ in principle can be extended to other tracers whose distributions that evolve in response to anthropogenic climate change. Furthermore, its implementation is such that in order to ~~decompose the change in a tracer, we require only high frequency~~ identify circulation driven changes in a given tracer requires only timeseries of the tracer in question, and a tracer which we may assume to change distribution only through redistribution~~:~~, for example C_{nat} ~~is a particularly useful tracer to this end~~. It should therefore also be applicable to observational timeseries with little modification.

Our globally integrated estimates indicate that the excess and redistributed temperature signals are currently of a similar size~~(Figure 1)~~, with excess temperature signals expected to exceed the redistributed temperature signals towards the end of the 2020's. This is in keeping with previous studies which find excess heat beginning to dominate over redistributed heat in the period 2011-2060 (Bronselaer and Zanna, 2020). Of course, as ~~we utilise~~ this is only one climate change run from a single model, there is a large uncertainty associated with this ~~.~~ and we recognise that it does not account for the spread of model responses to imposed climate change under an RCP8.5 scenario. However, our results are internally consistent, demonstrating a number of phenomena thought to occur under a changing climate explicitly in terms of the accumulation of excess heat and redistribution of preindustrial heat.

We have also produced, to our knowledge, the first modelled estimates of the redistribution of the preindustrial salinity field by the ocean and so the excess salinity field: that is, the changes in salinity due to changes in the balance of ~~evaporation and precipitation, rather than ocean~~ surface freshwater transport, directly excluding changes in ocean freshwater transport. By extension, we have also been able to produce ~~the first~~ estimates of excess and redistributed density~~. Curiously, we~~ , and so the contributions to steric sea level rise of temperature and salinity changes. We find that the penetration to depth of the ~~excess redistributed salinity and density signals are~~ redistributed salinity signal is far weaker than that of temperature, which, ~~particularly in the~~ with the exception of the North Atlantic, accounts for ~~the majority of deep warming~~a similar fraction of deep temperature change as the excess. However, we do find several signals in surface excess and redistributed salinity changes consistent with hydrological amplification, as well as a salinity signal in the South Atlantic as a previously identified 'salinity pile up' in the South Atlantic consistent with AMOC slowdown (Zhu and Liu, 2020). By the 2090's, the Southern and Subtropical North Atlantic show increasing redistributed surface salinity as a result of AMOC slowdown, with a decreasing redistributed salinity in the Subpolar North Atlantic. At the surface, we find that the majority of salinity change results from changes in E-P (excess), rather than circulation changes (redistributed), and that these patterns in excess salinity are consistent with both historical observations globally (Durack and Wijffels, 2010), and, in the Atlantic, with the salinity response to an idealised surface heat flux (Zika et al., 2018). We ~~also~~ find that the decrease in global mean excess salinity occurs earlier than the increase in globally integrated excess heat, consistent with previous studies which find significant ~~ice sheet~~ sea ice loss even in the early 20th century, before appreciable global warming ~~(Kjeldsen et al., 2015)~~(Wadhams and Munk, 2004), (Hetzinger et al., 2019). These results suggest that ~~whilst~~ historical observations of temperature changes are dominated by redistribution, with ~~the excess temperature only~~ excess temperature likely to dominate in the coming decades~~, historical~~ . Historical changes in salinity ~~may in fact~~ however may instead be predominately the result of excess salinity, rather than

redistribution. This holds at both global and local scales, with the patterns of local excess salinity appearing to be dominated by amplification of the hydrological cycle, and is in agreement with the findings of Stott et al. (2008), Terray et al. (2012), Pierce et al. (2012) and Skliris et al. (2014), who suggest the salinification of the subtropical North Atlantic and freshening of the Western Pacific Warm Pool may constitute an early fingerprint of anthropogenic forcings.

In applying our technique to the Atlantic, we have shown explicitly the redistribution of heat associated with changes to the overturning circulation, in addition to the aforementioned salinity signal. We also find fingerprints of AMOC change in both the redistributed temperature and salinity inventories of the North and South Atlantic: a large and rapid accumulation of negative ~~excess~~ redistributed heat in the North Atlantic over the period 2037-2099, as well as the accumulation of a large inventory of redistributed salinity in the South Atlantic over the same period. ~~We suggest that the application of this technique to historical observations may therefore help to constrain estimates of historical AMOC strength~~Over the period 2023-2099, for which the accumulation of excess heat in the North Atlantic is distinct from noise, we find 25±2% of global excess heat accumulation is in the North Atlantic. This is remarkably similar to observational estimates of anthropogenic carbon uptake (Sabine et al., 2004), again indicating the close relationship between excess heat and anthropogenic carbon.

Whilst by the end of the 21st century ~~temperature changes are expected to be~~ heat storage is dominated by excess ~~temperature, it is less clear for salinity that this will be the case: with the exception of a large increase in excess salinity in the Atlantic, excess salinity~~ heat, excess salinity estimates are largely uniform, and the contributions of redistributed and excess salinity to halosteric SLR are of similar scales in most locations (Figure ~~(6)): despite the indications that~~ 10). The only exception to this is a large increase in excess salinity in the Atlantic, This is despite patterns of regional change in ~~salinity appear to be~~ sea surface salinity and salinity inventory changes being dominated by the excess component, both historically and by the end of the 21st century. Though changes in salinity under anthropogenic climate change are expected to be less drastic than temperature, decomposing salinity into excess and redistributed components is also crucial to understanding the response of the ocean to global warming, due to its role in thermohaline circulation.

~~The decomposition of salinity also allows us to directly examine the dynamical forcing of excess and redistributed temperature and salinity.~~ By combining our estimates of excess temperature and salinity, we can directly compute the excess density change, and the redistribution of density. In the North Atlantic, we find warming and salinification in the excess components, and cooling and ~~freshing~~ freshening in the redistributed components. In both cases, these changes are in a density compensating fashion. Previous studies have noted that whilst density compensated water mass changes may be a general property of the ocean, the behaviour is particularly marked in the Atlantic (Lowe and Gregory, 2006), as well as important for contemporary Atlantic deep ocean heat uptake (Mauritzen et al., 2012), though it is uncertain how this will evolve. Our results suggest that ~~approximately density compensated~~ in the Atlantic, even by the last decade of our simulations, changes in excess temperature and salinity ~~remain important by the 2090's, though excess density generally acts to increase stratification: (negative) excess density generally decays quickly with depth~~act in a density compensating fashion. A consequence of this is that changes in surface freshwater fluxes associated with climate change oppose the reduction of overturning circulation associated with increased surface warming, ~~increasing the~~ opposing the reduction in the North Atlantic's capacity to sequester excess heat. This suggests that the excess contribution to ~~steric~~ themosteric SLR in the Atlantic will continue to grow on ~~the longest timescales.~~

centennial timescales, assuming continued CO_2 emissions, though the thermosteric SLR is greatly ameliorated by halosteric sea level fall. This is in agreement with historical observations (Antonov et al., 2002). However, the much smaller ~~redistributed~~ redistribution contribution to density indicates that changes to ocean circulation will have little effect on steric SLR in the North Atlantic ~~, and perhaps even act to ameliorate steric SLR. Finally,~~ by the end of the 21st century, although redistributed density compensation in the North Atlantic begins to break down in approximately 2050~~(Figure 2 (f))~~, as the redistribution of heat out of the North Atlantic significantly exceeds that of salinity by this time.

~~Globally, we find redistributed density inventories with scales approximately half the excess density inventory at most locations globally (Figure 6). As a result, the redistributed temperature and salinity fields have an associated effect on dynamics: the redistributed fields are dynamically active. Better understanding the feedback of redistributed fields on dynamics may therefore prove a useful tool in understanding timescales for future ocean circulation change associated with anthropogenic climate change.~~

Finally, although only being applied within a single model, our patterns of excess and redistributed heat storage are consistent with previous studies ~~(Bronselaer and Zanna, 2020), (Winton et al., 2013), (Banks and Gregory, 2006)~~ (Winton et al., 2013), (Bronselaer and Zanna, 2020), (Williams et al., 2021), despite differing assumptions used in the calculation of the redistribution of heat from carbon. ~~We have also shown that this technique can be considered, in the case of temperature, to be the opposite limit of a generalised relationship between temperature and carbon change used in previous studies.~~ A key benefit of the method introduced here compared to prior carbon based estimates of circulation change is that it ~~can be used to estimate the redistribution of a suite of tracers as it relies only on spatial information, and it does not necessarily require estimates of global mean quantities~~is applicable both to observations and multiple tracers. In combination with other techniques, we believe this method to be a powerful tool for understanding ~~the mechanistic drivers of changes to~~ causes of future ocean temperature, salinity and density change. ~~Though particularly useful for understanding future sea level rise, it may also have important uses for understanding the future transport of salinity and carbon by sea ice(Moreau et al., 2016), sequestration of carbon by the ocean (Frölicher et al., 2015) and northwards heat transport of the Atlantic (Lowe and Gregory, 2006),(Mauritzen et al., 2012)~~ .

Code and data availability. The model output we use as well as the code used to decompose the temperature and salinity fields are available upon request. Core functionality for the decomposition is freely available at https://github.com/charles-turner-1/temp_decomp.

Appendix A: Uncertainty in estimates of local redistribution

We estimate a local gradient, $\Delta\Theta/\Delta C_{\mathrm{nat}}$ or $\Delta S/\Delta C_{\mathrm{nat}}$ by applying two dimensional PCA to the ~~raw data: timeseries of~~ timeseries of yearly deviations of the two variables ~~at a point. We choose this indirect statistical approach as it is applicable to both models and observations: attempting to calculate κ_s directly is only possible with full, 3 dimensional velocity fields,~~

~~which do not exist for observations~~from their decadal mean values at each grid cell. This is equivalent to performing a total least squares fit to obtain a linear relationship between the two variables.

We then scale the data to normalise the ranges of Θ/S and C_{nat} before again performing ~~PCA~~ 2D PCA on our timeseries at each grid cell to estimate the fraction of the covariance contained within each principle component. This yields the fraction of the total variance explained by each principal component, which we refer to as ε_1 and ε_2: these can be thought of the axes of an ellipse describing ~~our scatter cloud~~ a scatter cloud relating the two variables. A fit which is a perfect line can be thought of as the limit of this ellipse where $\varepsilon_1 \to 1$ and $\varepsilon_2 \to 0$. Conversely, an essentially random fit through a spherical cloud of points can be thought of as the case where $\varepsilon_1 = \varepsilon_2$.

We use the eccentricity of this ellipse as a suppression factor, ~~S_u: ϕ_u~~:

$$S\phi_u = \sqrt{1 - \left(\frac{\varepsilon_2}{\varepsilon_1}\right)^2} \tag{A1}$$

The need for conservative estimates of confidence in the fit is particularly important for fits in which no discernable correlation can be drawn: for these, gradients associating minor changes in C_{nat} with large changes in Θ or S can be obtained, effectively at random, and so our suppression factor must remove these effectively. As we concern ourselves primarily with inventories, this approach was found to be preferable to including large uncertainties due to a small number of spurious points, or simply setting a threshold below which we do not attempt to diagnose the redistribution of heat. Only 6% of ε_1 values are scaled by a factor of $1/2$ or less: this was found to be a suitable compromise, with only the most unreliable estimates strongly suppressed.

~~Approximately 80% of grid cells globally have an eccentricity of 0.8-1, and we find by the end of our run, the suppression factor alters the redistributed temperature of 93% grid cells globally by less than 0.04 degrees, and 60% by less than 0.02 degrees, though the RMS mean redistributed temperature is reduced by 5%. However, the small number of grid cells producing extremely large estimates (10's of degrees of change) are effectively suppressed. We therefore estimate that the statistical nature of our method introduces an error of approximately 5% into our inventories.~~ Alternative methods may produce better quantifications of uncertainty, though are not considered here as the eccentricity method was sufficient for our purposes.

We then calculate the redistribution coefficient κ_r as

$$\kappa_r = S\phi_u \times \kappa_s \tag{A2}$$

The implementation of this is demonstrated in Figure A1, for two points in the North Atlantic at approximately 24~~North, 30W~~ °N, 30°W and 850m and 1950m. The poorly correlated point, Figure A1a and A1c, is an extreme outlier, shown for demonstrative purposes. Here the fit is essentially random, and so estimates of temperature redistribution are scaled to reflect this uncertainty: the eccentricity of the ellipse described by the cloud of points in $\Theta - C_{nat}$ space is used as a scale factor. For ~~a~~ the strongly correlated point, shown in panels (b) and (d), temperature and C_{nat} variability are almost perfectly anticorrelated, representing the dominance of vertical ~~heave and shoal~~ structure in determining the redistribution coefficient ~~κ_r~~κ_r^T. Here, ~~$\kappa_r = -0.0210$~~$\kappa_r^T = -0.0210$, $\partial_z\Theta/\partial_z \mathrm{DIC} = -0.0208$. ~~The strongly correlated point also demonstrates how our parallel velocities restraint is greatly relaxed in practice: horizontal gradients at this location are small (or they would contribute to κ_r), and so horizontal circulatory changes will not contribute strongly to temperature redistribution, even if our condition~~

on parallel velocities ($\mathbf{v}_s \parallel \mathbf{v}_l$) is not well satisfied. In Figure A1, the technique is demonstrated using monthly mean data for visibility, though we use yearly mean data when producing our estimates.

Appendix B: Merging one and two step estimates

Our estimation technique assumes that the relationship between short timescale changes is dominated by circulation variability. However, at the surface, changes in salinity and $\mathrm{C_{nat}}$ are instead dominated by freshwater fluxes: an excess of evaporation over precipitation will increase concentrations of salt and $\mathrm{C_{nat}}$, coupling changes in the two. This leads to changes which are properly described as excess salinity being partitioned into redistributed salinity.

To account for this, we use a two step estimation process. Equation 15 states that we may estimate the redistribution in an arbitrary tracer Q, provided that $\mathrm{C_{nat}}$ changes only due to redistribution:

$$\frac{dQ_r}{d\mathrm{C_{nat}}} = \frac{\mathbf{v}_l \cdot \nabla Q}{\mathbf{v}_l \cdot \nabla \mathrm{C_{nat}}}$$

As we note, we may combine Equations 7 & 8 in order to estimate redistributed salinity from redistributed temperature, or vice versa. We therefore estimate excess salinity at the surface as

$$\Delta S_r = \kappa_r^{\mathrm{T-S}} \times \Delta\Theta_r, \tag{B1}$$

However, estimations of this nature are not limited simply to $\mathrm{C_{nat}}$: we may use any tracer which changes only through redistribution. We utilise this by using temperature redistribution in the upper 200m to estimate salinity redistribution. The same approach is applied not to the $\Theta - \mathrm{C_{nat}}$ or $S - \mathrm{C_{nat}}$ curve, but the T-S curve, and the redistributed salinity is then estimated from this :

$$\Delta S_r = \frac{\mathbf{v} \cdot \nabla S}{\mathbf{v} \cdot \nabla \Theta} \Delta\Theta_r$$

where $\kappa_r^{\mathrm{T-S}}$ is an estimate of the local slope of the temperature-salinity curve, produced in the same fashion as our previous estimates. We refer to this estimate of surface excess salinity as a two step estimate.

We then merge the two estimates using a sigmoidal weighting scheme based on depth. Our simulations use 64 vertical levels, with the 20th level corresponding to approximately 200m. Denoting the i$^{\mathrm{th}}$ vertical level z_i, the one step estimate as S_1 and the two step estimate as S_2, we calculate our final estimate of salinity redistribution, S, as

$$S = S_1 \times \sigma\left(\frac{z_i + 20}{2}\right) + S_2 \times \left(1 - \sigma\left(\frac{z_i + 20}{2}\right)\right), \tag{B2}$$

where $\sigma(z)$ is the sigmoid function:

$$\sigma(z) = \frac{1}{1 + e^{-z}} \tag{B3}$$

Appendix C: Gamma Factor

Figure C1 shows the γ factor over our full run. It increases from 0 at the beginning of the run to 0.117 by 2099. We perform smoothing as in the late 19th and early 20th century, C_{anth} inventories are small and so large corrections are necessary to perfectly correct a small amount of C_{sat} outgassing: smoothing removes this effectively. By the 21st century, C_{anth} inventories are large enough that smoothing has little effect. Finally, we note that the γ factor does not begin to increase significantly until the late 20th century, approximately the same time that globally integrated ocean heat content begins to increase. Thus, to first order, γ corrects for C_{sat} outgassing due to ocean warming.

Author contributions. CT designed the technique for temperature decomposition, and EM realised the extensibility to salinity. All authors contributed to interpretation and writing the manuscript.

Competing interests. The authors declare no competing interests

Acknowledgements. We would like to thank Matthew Couldrey for kindly allowing us to use his simulations for this research. EM, PB were supported by Natural Environment Research Council grant NE/P019293/1 (TICTOC) CT was supported by the Natural Environmental Research Council [grant number NE/L002531/1]

References

Antonov, J. I., Levitus, S., and Boyer, T. P.: Steric sea level variations during 1957–1994: Importance of salinity, Journal of Geophysical Research: Oceans, 107, SRF 14–1–SRF 14–8, https://doi.org/https://doi.org/10.1029/2001JC000964, 2002.

Banks, H. T. and Gregory, J. M.: Mechanisms of ocean heat uptake in a coupled climate model and the implications for tracer based predictions of ocean heat uptake, Geophysical Research Letters, 33, https://doi.org/https://doi.org/10.1029/2005GL025352, 2006.

Bindoff, N. L. and Mcdougall, T. J.: Diagnosing Climate Change and Ocean Ventilation Using Hydrographic Data, Journal of Physical Oceanography, 24, 1137 – 1152, https://doi.org/10.1175/1520-0485(1994)024<1137:DCCAOV>2.0.CO;2, 1994.

Bopp, L., Lévy, M., Resplandy, L., and Sallée, J. B.: Pathways of anthropogenic carbon subduction in the global ocean, Geophysical Research Letters, 42, 6416–6423, https://doi.org/https://doi.org/10.1002/2015GL065073, 2015.

Bronselaer, B. and Zanna, L.: Heat and carbon coupling reveals ocean warming due to circulation changes, Nature, 584, 227–233, https://doi.org/10.1038/s41586-020-2573-5, 2020.

Caesar, L., Rahmstorf, S., Robinson, A., Feulner, G., and Saba, V.: Observed fingerprint of a weakening Atlantic Ocean overturning circulation, Nature, 556, 191–196, https://doi.org/10.1038/s41586-018-0006-5, 2018.

Church, J., Clark, P., Cazenave, A., Gregory, J., Jevrejeva, S., Levermann, A., Merrifield, M., Milne, G., Nerem, R., Nunn, P., Payne, A., Pfeffer, W., Stammer, D., and Unnikrishnan, A.: Sea Level Change, in: Climate Change 2013: The Physical Science Basis. Contribution of Working Group I to the Fifth Assessment Report of the Intergovernmental Panel on Climate Change, edited by Stocker, T., Qin, D., Plattner, G.-K., Tignor, M., Allen, S., Boschung, J., Nauels, A., Xia, Y., Bex, V., and Midgley, P., pp. 1137–1216, Cambridge University Press, https://doi.org/10.1017/CBO9781107415324.026, section: 13 Type: Book Section, 2013.

Church, J. A., White, N. J., Konikow, L. F., Domingues, C. M., Cogley, J. G., Rignot, E., Gregory, J. M., van den Broeke, M. R., Monaghan, A. J., and Velicogna, I.: Revisiting the Earth's sea-level and energy budgets from 1961 to 2008, Geophysical Research Letters, 38, https://doi.org/https://doi.org/10.1029/2011GL048794, 2011.

Collins, W. J., Bellouin, N., Doutriaux-Boucher, M., Gedney, N., Halloran, P., Hinton, T., Hughes, J., Jones, C. D., Joshi, M., Liddicoat, S., Martin, G., O'Connor, F., Rae, J., Senior, C., Sitch, S., Totterdell, I., Wiltshire, A., and Woodward, S.: Development and evaluation of an Earth-System model – HadGEM2, Geoscientific Model Development, 4, 1051–1075, https://doi.org/10.5194/gmd-4-1051-2011, 2011.

Couldrey, M. P., Oliver, K. I. C., Yool, A., Halloran, P. R., and Achterberg, E. P.: On which timescales do gas transfer velocities control North Atlantic CO2 flux variability?, Global Biogeochemical Cycles, 30, 787–802, https://doi.org/https://doi.org/10.1002/2015GB005267, 2016.

Couldrey, M. P., Oliver, K. I. C., Yool, A., Halloran, P. R., and Achterberg, E. P.: Drivers of 21$^{\mathrm{st}}$ Century carbon cycle variability in the North Atlantic Ocean, Biogeosciences Discussions, 2019, 1–33, https://doi.org/10.5194/bg-2019-16, 2019.

Desbruyères, D., McDonagh, E. L., King, B. A., and Thierry, V.: Global and Full-Depth Ocean Temperature Trends during the Early Twenty-First Century from Argo and Repeat Hydrography, Journal of Climate, 30, 1985 – 1997, https://doi.org/10.1175/JCLI-D-16-0396.1, 2017.

Durack, P. J. and Wijffels, S. E.: Fifty-Year Trends in Global Ocean Salinities and Their Relationship to Broad-Scale Warming, Journal of Climate, 23, 4342 – 4362, https://doi.org/10.1175/2010JCLI3377.1, 2010.

Firing, Y. L., McDonagh, E. L., King, B. A., and Desbruyères, D. G.: Deep temperature variability in Drake Passage, Journal of Geophysical Research: Oceans, 122, 713–725, https://doi.org/https://doi.org/10.1002/2016JC012452, 2017.

Frölicher, T. L., Sarmiento, J. L., Paynter, D. J., Dunne, J. P., Krasting, J. P., and Winton, M.: Dominance of the Southern Ocean in Anthropogenic Carbon and Heat Uptake in CMIP5 Models, Journal of Climate, 28, 862 – 886, https://doi.org/10.1175/JCLI-D-14-00117.1, 2015.

Goodwin, P., Williams, R. G., and Ridgwell, A.: Sensitivity of climate to cumulative carbon emissions due to compensation of ocean heat and carbon uptake, Nature Geoscience, 8, 29–34, https://doi.org/10.1038/ngeo2304, 2015.

Gould, W. J. and Cunningham, S. A.: Global-scale patterns of observed sea surface salinity intensified since the 1870s, Communications Earth & Environment, 2, 76, https://doi.org/10.1038/s43247-021-00161-3, 2021.

Gregory, J. M., Bouttes, N., Griffies, S. M., Haak, H., Hurlin, W. J., Jungclaus, J., Kelley, M., Lee, W. G., Marshall, J., Romanou, A., Saenko, O. A., Stammer, D., and Winton, M.: The Flux-Anomaly-Forced Model Intercomparison Project (FAFMIP) contribution to CMIP6: investigation of sea-level and ocean climate change in response to CO_2 forcing, Geoscientific Model Development, 9, 3993–4017, https://doi.org/10.5194/gmd-9-3993-2016, 2016.

Gruber, N.: Warming up, turning sour, losing breath: ocean biogeochemistry under global change, Philosophical Transactions of the Royal Society A: Mathematical, Physical and Engineering Sciences, 369, 1980–1996, https://doi.org/10.1098/rsta.2011.0003, 2011.

Gruber, N., Sarmiento, J. L., and Stocker, T. F.: An improved method for detecting anthropogenic CO2 in the oceans, Global Biogeochemical Cycles, 10, 809–837, https://doi.org/https://doi.org/10.1029/96GB01608, 1996.

Hall, T. M., Haine, T. W. N., and Waugh, D. W.: Inferring the concentration of anthropogenic carbon in the ocean from tracers, Global Biogeochemical Cycles, 16, 78–1–78–15, https://doi.org/https://doi.org/10.1029/2001GB001835, 2002.

Hetzinger, S., Halfar, J., Zajacz, Z., and Wisshak, M.: Early start of 20th-century Arctic sea-ice decline recorded in Svalbard coralline algae, Geology, 47, 963–967, https://doi.org/10.1130/G46507.1, 2019.

Hinkel, J., Lincke, D., Vafeidis, A. T., Perrette, M., Nicholls, R. J., Tol, R. S. J., Marzeion, B., Fettweis, X., Ionescu, C., and Levermann, A.: Coastal flood damage and adaptation costs under 21st century sea-level rise, Proceedings of the National Academy of Sciences, 111, 3292–3297, https://doi.org/10.1073/pnas.1222469111, 2014.

Johns, W. E., Baringer, M. O., Beal, L. M., Cunningham, S. A., Kanzow, T., Bryden, H. L., Hirschi, J. J. M., Marotzke, J., Meinen, C. S., Shaw, B., and Curry, R.: Continuous, Array-Based Estimates of Atlantic Ocean Heat Transport at 26.5°N, Journal of Climate, 24, 2429 – 2449, https://doi.org/10.1175/2010JCLI3997.1, 2011.

Katavouta, A., Williams, R. G., Goodwin, P., and Roussenov, V.: Reconciling Atmospheric and Oceanic Views of the Transient Climate Response to Emissions, Geophysical Research Letters, 45, 6205–6214, https://doi.org/https://doi.org/10.1029/2018GL077849, 2018.

Khatiwala, S., Visbeck, M., and Cane, M. A.: Accelerated simulation of passive tracers in ocean circulation models, Ocean Modelling, 9, 51–69, https://doi.org/https://doi.org/10.1016/j.ocemod.2004.04.002, 2005.

Khatiwala, S., Tanhua, T., Mikaloff Fletcher, S., Gerber, M., Doney, S. C., Graven, H. D., Gruber, N., McKinley, G. A., Murata, A., Ríos, A. F., and Sabine, C. L.: Global ocean storage of anthropogenic carbon, Biogeosciences, 10, 2169–2191, https://doi.org/10.5194/bg-10-2169-2013, 2013.

Kjeldsen, K., Korsgaard, N., Bjørk, A., Khan, S., Box, J., Funder, S., Larsen, N., Bamber, J., Colgan, W., van den Broeke, M., Siggaard-Andersen, M.-L., Nuth, C., Schomacker, A., Andresen, C., Willerslev, E., and Kjær, K.: Spatial and temporal distribution of mass loss from the Greenland Ice Sheet since AD 1900, Nature, 528, 396–400, https://doi.org/10.1038/nature16183, 2015.

Lauvset, S. K., Key, R. M., Olsen, A., van Heuven, S., Velo, A., Lin, X., Schirnick, C., Kozyr, A., Tanhua, T., Hoppema, M., Jutterström, S., Steinfeldt, R., Jeansson, E., Ishii, M., Perez, F. F., Suzuki, T., and Watelet, S.: A new global interior ocean mapped climatology: the $1^\circ \times 1^\circ$ GLODAP version 2, Earth System Science Data, 8, 325–340, https://doi.org/10.5194/essd-8-325-2016, 2016.

Levang, S. J. and Schmitt, R. W.: Centennial Changes of the Global Water Cycle in CMIP5 Models, Journal of Climate, 28, 6489 – 6502, https://doi.org/10.1175/JCLI-D-15-0143.1, 2015.

Lowe, J. A. and Gregory, J. M.: Understanding projections of sea level rise in a Hadley Centre coupled climate model, Journal of Geophysical Research: Oceans, 111, https://doi.org/https://doi.org/10.1029/2005JC003421, 2006.

MacDougall, A. H. and Friedlingstein, P.: The Origin and Limits of the Near Proportionality between Climate Warming and Cumulative CO 2 Emissions , Journal of Climate, 28, 4217–4230, https://doi.org/10.1175/jcli-d-14-00036.1, 2015.

Madec, G.: NEMO ocean engine, https://doi.org/10.5281/zenodo.1464816, 2008.

Madec, G. and Imbard, M.: A global ocean mesh to overcome the North Pole singularity, Climate Dynamics, 12, 381–388, 1996.

Martin, T. H. D. T. G. M., Bellouin, N., Collins, W. J., Culverwell, I. D., Halloran, P. R., Hardiman, S. C., Hinton, T. J., Jones, C. D., McDonald, R. E., McLaren, A. J., O'Connor, F. M., Roberts, M. J., Rodriguez, J. M., Woodward, S., Best, M. J., Brooks, M. E., Brown, A. R., Butchart, N., Dearden, C., Derbyshire, S. H., Dharssi, I., Doutriaux-Boucher, M., Edwards, J. M., Falloon, P. D., Gedney, N., Gray, L. J., Hewitt, H. T., Hobson, M., Huddleston, M. R., Hughes, J., Ineson, S., Ingram, W. J., James, P. M., Johns, T. C., Johnson, C. E., Jones, A., Jones, C. P., Joshi, M. M., Keen, A. B., Liddicoat, S., Lock, A. P., Maidens, A. V., Manners, J. C., Milton, S. F., Rae, J. G. L., Ridley, J. K., Sellar, A., Senior, C. A., Totterdell, I. J., Verhoef, A., Vidale, P. L., and Wiltshire, A.: The HadGEM2 family of Met Office Unified Model climate configurations, Geoscientific Model Development, 4, 723–757, https://doi.org/10.5194/gmd-4-723-2011, 2011.

Mauritzen, C., Melsom, A., and Sutton, R. T.: Importance of density-compensated temperature change for deep North Atlantic Ocean heat uptake, Nature Geoscience, 5, 905–910, https://doi.org/10.1038/ngeo1639, 2012.

McDougall, T. J. and Barker, P. M.: Getting started with TEOS-10 and the Gibbs Seawater (GSW) Oceanographic Toolbox, SCOR/IAPSO WG127, p. 28, 2011.

McKinley, G. A., Fay, A. R., Lovenduski, N. S., and Pilcher, D. J.: Natural Variability and Anthropogenic Trends in the Ocean Carbon Sink, Annual Review of Marine Science, 9, 125–150, https://doi.org/10.1146/annurev-marine-010816-060529, pMID: 27620831, 2017.

Moreau, S., Vancoppenolle, M., Bopp, L., Aumont, O., Madec, G., Delille, B., Tison, J.-L., Barriat, P.-Y., and Goosse, H.: Assessment of the sea-ice carbon pump: Insights from a three-dimensional ocean-sea-ice biogeochemical model (NEMO-LIM-PISCES), Elementa: Science of the Anthropocene, 4, https://doi.org/10.12952/journal.elementa.000122, 000122, 2016.

Oschlies, A., Brandt, P., Stramma, L., and Schmidtko, S.: Drivers and mechanisms of ocean deoxygenation, Nature Geoscience, 11, 467–473, https://doi.org/10.1038/s41561-018-0152-2, 2018.

Pardaens, A. K., Lowe, J. A., Brown, S., Nicholls, R. J., and de Gusmão, D.: Sea-level rise and impacts projections under a future scenario with large greenhouse gas emission reductions, Geophysical Research Letters, 38, https://doi.org/https://doi.org/10.1029/2011GL047678, 2011.

Pierce, D. W., Gleckler, P. J., Barnett, T. P., Santer, B. D., and Durack, P. J.: The fingerprint of human-induced changes in the ocean's salinity and temperature fields, Geophysical Research Letters, 39, https://doi.org/https://doi.org/10.1029/2012GL053389, 2012.

Riahi, K., Rao, S., Krey, V., Cho, C., Chirkov, V., Fischer, G., Kindermann, G., Nakicenovic, N., and Rafaj, P.: RCP 8.5—A scenario of comparatively high greenhouse gas emissions, Climatic Change, 109, 33–57, https://doi.org/10.1007/s10584-011-0149-y, 2011.

Rodgers, K. B., Ishii, M., Frölicher, T. L., Schlunegger, S., Aumont, O., Toyama, K., and Slater, R. D.: Coupling of Surface Ocean Heat and Carbon Perturbations over the Subtropical Cells under Twenty-First Century Climate Change, Journal of Climate, 33, 10 321 – 10 338, https://doi.org/10.1175/JCLI-D-19-1022.1, 2020.

Sabine, C., Feely, R., Gruber, N., Key, R., Lee, K., Bullister, J., Wanninkhof, R., Wong, C., Wallace, D., Tilbrook, B., Millero, F., Peng, T.-H., Kozyr, A., Ono, T., and Rios, A.: The Oceanic Sink for Anthropogenic CO2, Science (New York, N.Y.), 305, 367–71, https://doi.org/10.1126/science.1097403, 2004.

Sathyanarayanan, A., Kohl, A., and Stammer, D.: Ocean Salinity changes in the global ocean under global warming conditions Part 1: Mechanisms in a strong warming scenario, Journal of Climate, pp. 1 – 56, https://doi.org/10.1175/JCLI-D-20-0865.1, 2021.

Schwinger, J., Tjiputra, J. F., Heinze, C., Bopp, L., Christian, J. R., Gehlen, M., Ilyina, T., Jones, C. D., Salas-Mélia, D., Segschneider, J., Séférian, R., and Totterdell, I.: Nonlinearity of ocean carbon cycle feedbacks in CMIP5 earth system models, Journal of Climate, 27, 3869–3888, https://doi.org/10.1175/JCLI-D-13-00452.1, 2014.

Sgubin, G., Swingedouw, D., Drijfhout, S., Hagemann, S., and Robertson, E.: Multimodel analysis on the response of the AMOC under an increase of radiative forcing and its symmetrical reversal, Climate Dynamics, 45, https://doi.org/10.1007/s00382-014-2391-2, 2014.

Skliris, N., Marsh, R., Josey, S. A., Good, S. A., Liu, C., and Allan, R. P.: Salinity changes in the World Ocean since 1950 in relation to changing surface freshwater fluxes, Climate Dynamics, 43, 709–736, https://doi.org/10.1007/s00382-014-2131-7, 2014.

Stott, P. A., Sutton, R. T., and Smith, D. M.: Detection and attribution of Atlantic salinity changes, Geophysical Research Letters, 35, https://doi.org/https://doi.org/10.1029/2008GL035874, 2008.

Terray, L., Corre, L., Cravatte, S., Delcroix, T., Reverdin, G., and Ribes, A.: Near-Surface Salinity as Nature's Rain Gauge to Detect Human Influence on the Tropical Water Cycle, Journal of Climate, 25, 958 – 977, https://doi.org/10.1175/JCLI-D-10-05025.1, 2012.

Thomas, J., Waugh, D., and Gnanadesikan, A.: Relationship between Ocean Carbon and Heat Multidecadal Variability, Journal of Climate, 31, 1467 – 1482, https://doi.org/10.1175/JCLI-D-17-0134.1, 2018.

Timmermann, R., Goosse, H., Madec, G., Fichefet, T., Ethe, C., and Dulière, V.: On the representation of high latitude processes in the ORCA-LIM global coupled sea ice–ocean model, Ocean Modelling, 8, 175–201, 2005.

Touratier, F. and Goyet, C.: Definition, properties, and Atlantic Ocean distribution of the new tracer TrOCA, Journal of Marine Systems, 46, 169–179, https://doi.org/https://doi.org/10.1016/j.jmarsys.2003.11.016, 2004.

Vázquez-Rodríguez, M., Padin, X. A., Ríos, A. F., Bellerby, R. G. J., and Pérez, F. F.: An upgraded carbon-based method to estimate the anthropogenic fraction of dissolved CO_2 in the Atlantic Ocean, Biogeosciences Discussions, 6, 4527–4571, https://doi.org/10.5194/bgd-6-4527-2009, 2009.

Wadhams, P. and Munk, W.: Ocean freshening, sea level rising, sea ice melting, Geophysical Research Letters, 31, https://doi.org/https://doi.org/10.1029/2004GL020039, 2004.

Weaver, A. J., Sedláček, J., Eby, M., Alexander, K., Crespin, E., Fichefet, T., Philippon-Berthier, G., Joos, F., Kawamiya, M., Matsumoto, K., Steinacher, M., Tachiiri, K., Tokos, K., Yoshimori, M., and Zickfeld, K.: Stability of the Atlantic meridional overturning circulation: A model intercomparison, Geophysical Research Letters, 39, https://doi.org/https://doi.org/10.1029/2012GL053763, 2012.

Williams, R. G. and Follows, M. J.: Ocean Dynamics and the Carbon Cycle: Principles and Mechanisms, Cambridge University Press, https://doi.org/10.1017/CBO9780511977817, 2011.

Williams, R. G., Katavouta, A., and Roussenov, V.: Regional Asymmetries in Ocean Heat and Carbon Storage due to Dynamic Redistribution in Climate Model Projections, Journal of Climate, 34, 3907 – 3925, https://doi.org/10.1175/JCLI-D-20-0519.1, 2021.

Winton, M., Griffies, S. M., Samuels, B. L., Sarmiento, J. L., and Frölicher, T. L.: Connecting Changing Ocean Circulation with Changing Climate, Journal of Climate, 26, 2268 – 2278, https://doi.org/10.1175/JCLI-D-12-00296.1, 2013.

Yool, A., Popova, E. E., and Anderson, T. R.: MEDUSA-2.0: an intermediate complexity biogeochemical model of the marine carbon cycle for climate change and ocean acidification studies, Geoscientific Model Development, 6, 1767–1811, https://doi.org/10.5194/gmd-6-1767-2013, 2013.

Zanna, L., Khatiwala, S., Gregory, J. M., Ison, J., and Heimbach, P.: Global reconstruction of historical ocean heat storage and transport, Proceedings of the National Academy of Sciences, 116, 1126–1131, 2019.

Zhu, C. and Liu, Z.: Weakening Atlantic overturning circulation causes South Atlantic salinity pile-up, Nature Climate Change, 10, 998–1003, https://doi.org/10.1038/s41558-020-0897-7, 2020.

Zika, J. D., Skliris, N., Blaker, A. T., Marsh, R., Nurser, A. J. G., and Josey, S. A.: Improved estimates of water cycle change from ocean salinity: the key role of ocean warming, Environmental Research Letters, 13, 074 036, https://doi.org/10.1088/1748-9326/aace42, 2018.

Zika, J. D., Gregory, J. M., McDonagh, E. L., Marzocchi, A., and Clément, L.: Recent Water Mass Changes Reveal Mechanisms of Ocean Warming, Journal of Climate, 34, 3461 – 3479, https://doi.org/10.1175/JCLI-D-20-0355.1, 2021.

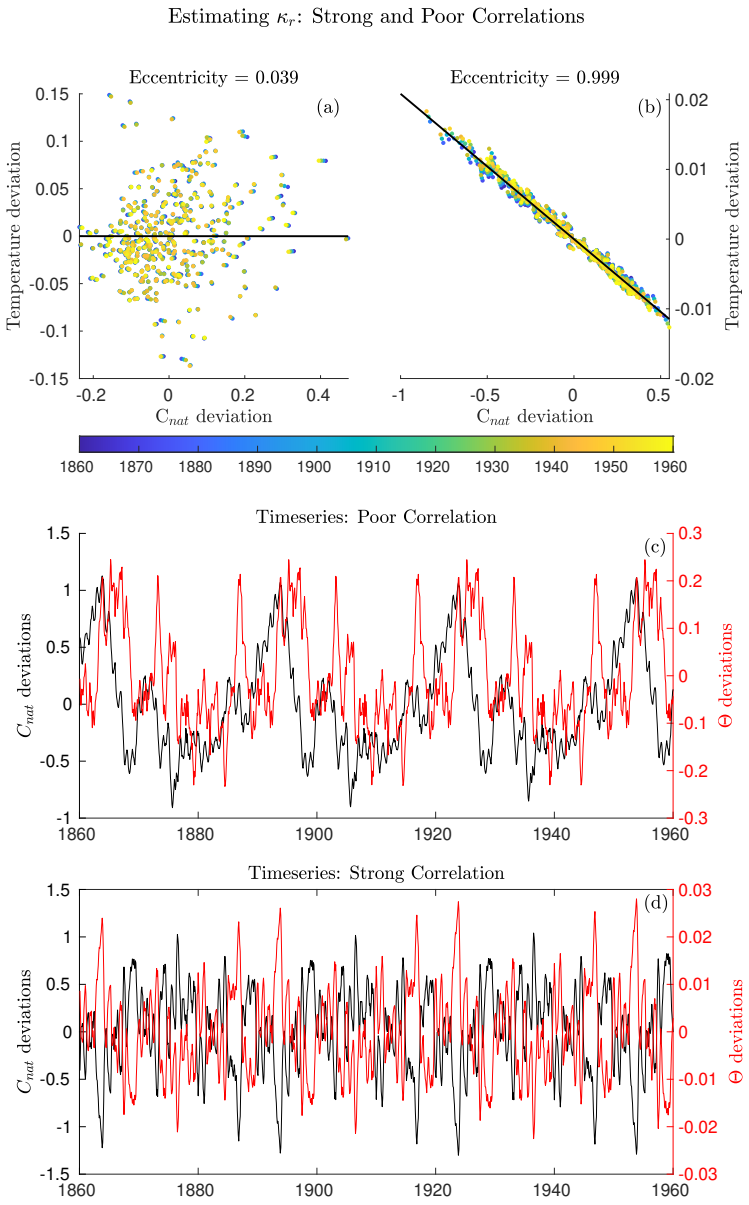

Figure A1. The correlations between $\mathrm{C_{nat}}$ and Θ used to establish a κ_r value, for a poorly correlated point ((a),(c)), and a well correlated point ((b),(d)), in $\Theta - \mathrm{C_{nat}}$ space ((a), (b)), and timeseries of both ((c),(d)). These two points are located at 24N,30W in the Atlantic, at depths of 850 and 1950m. The major axis of the covariance ellipse in panels (a) and (b) is shown in black.

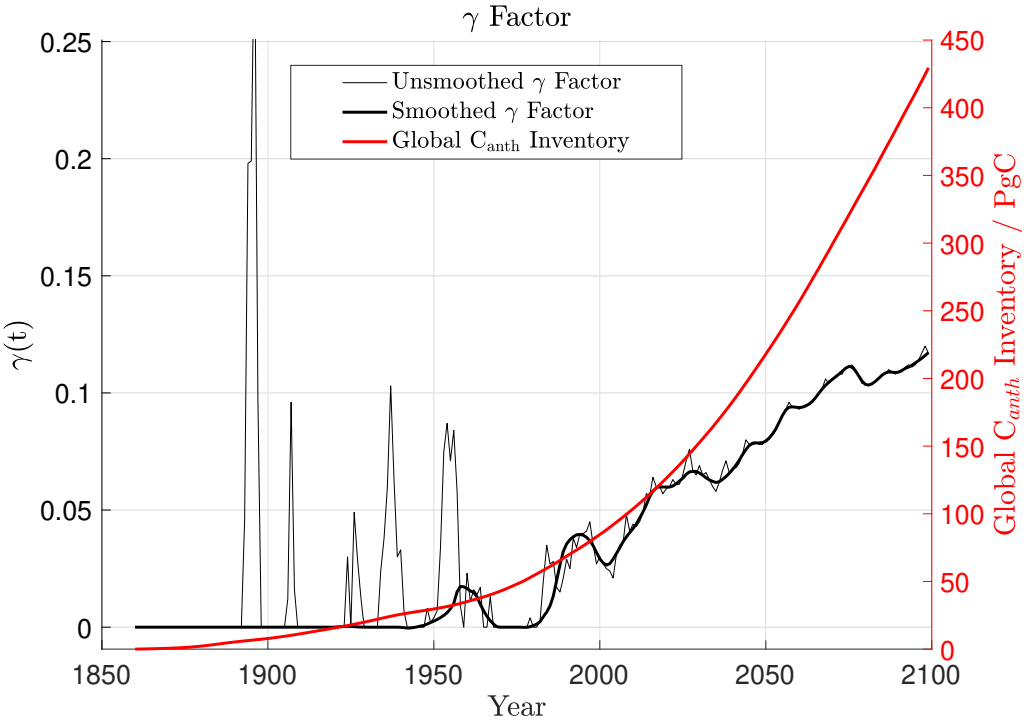

Figure C1. The calculated γ factor (thin black line), smoothed γ factor (thick black line), and global anthropogenic carbon inventory (red line)(.